Available online at www.sciencedirect.com

ScienceDirect

Geochimica et Cosmochimica Acta 203 (2017) 364–380

Geochimica et Cosmochimica Acta

www.elsevier.com/locate/gca

Combined ^{34}S, ^{33}S and ^{18}O isotope fractionations record different intracellular steps of microbial sulfate reduction

Gilad Antler [a,b,*], Alexandra V. Turchyn [a], Shuhei Ono [c], Orit Sivan [d], Tanja Bosak [c]

[a] Department of Earth Sciences, University of Cambridge, Cambridge CB2 3EQ, UK
[b] Center for Geomicrobiology, Department of Biological Sciences, Aarhus University, Ny Munkegade, Bld. 1535, 8000 Aarhus C, Denmark
[c] Department of Earth, Atmospheric and Planetary Sciences, Massachusetts Institute of Technology, Cambridge, MA 02139, USA
[d] Department of Geological and Environmental Sciences, Ben-Gurion University of the Negev, P. O. Box 653, Beer-Sheva 84105, Israel

Received 4 April 2016; accepted in revised form 10 January 2017; available online 18 January 2017

Abstract

Several enzymatic steps in microbial sulfate reduction (MSR) fractionate the isotope ratios of $^{33}S/^{32}S$, $^{34}S/^{32}S$ and $^{18}O/^{16}O$ in extracellular sulfate, but the effects of different intracellular processes on the isotopic composition of residual sulfate are still not well quantified. We measured combined multiple sulfur ($^{33}S/^{32}S$, $^{34}S/^{32}S$) and oxygen ($^{18}O/^{16}O$) isotope ratios of sulfate in pure cultures of a marine sulfate reducing bacterium *Desulfovibrio* sp. DMSS-1 grown on different organic substrates. These measurements are consistent with the previously reported correlations of oxygen and sulfur isotope fractionations with the cell-specific rate of MSR: faster reduction rates produced smaller isotopic fractionations for all isotopes. Combined isotope fractionation of oxygen and multiple sulfur isotopes are also consistent with the relationship between the rate limiting step during microbial sulfate reduction and the availability of the DsrC subunit. These experiments help reconstruct and interpret processes that operate in natural pore waters characterized by high $^{18}O/^{16}O$ and moderate $^{34}S/^{32}S$ ratios and suggest that some multiple isotope signals in the environment cannot be explained by microbial sulfate reduction alone. Instead, these signals support the presence of active, but slow sulfate reduction as well as the reoxidation of sulfide.

Keywords: Microbial sulfate reduction; Sulfur isotopes; Oxygen isotopes; Multiple sulfur isotopes; Anaerobic respiration

1. INTRODUCTION

Microbial sulfate reduction (MSR) is key process in the global carbon cycle, responsible for the oxidation of a substantial fraction of organic matter that reaches marine sediments (Kasten and Jørgensen, 2000; Bowles et al., 2014). The biochemical steps during MSR have been studied for more than 60 years (e.g. Hilz and Lipmann, 1955; Pierik et al., 1992; Oliveira et al., 2008; Santos et al., 2015). The reduction of sulfate is thought to occur in five major metabolic steps (Fig. 1). During the first step, extracellular sulfate is transported into the cytoplasm by sulfate permeases (Piłsyk and Paszewski, 2009). In the second step (step 2), intracellular sulfate is activated with adenosine triphosphate to form adenosine 5′ phosphosulfate (APS) (Hilz and Lipmann, 1955) by ATP sulfurylase (Michaels et al., 1970). In the third step (step 3), the APS is reduced to sulfite (SO_3^{2-}). In the fourth step (step 4), sulfite reduced to sulfide by dissimilatory sulfide reductase (Dsr) with two key subunits (DsrAB and DsrC) but also can be reduced to a variety of sulfur intermediates such as elemental sulfur (S°), trithionate ($S_4O_6^{2-}$) and thiosulfate ($S_2O_3^{-2}$) (e.g. Kobayashi et al., 1969; Fitz and Cypionka, 1990; Akagi, 1995; Bradley et al., 2011). It was recently shown that these intermediates can form *in vitro* in the presence of excess

* Corresponding authors at: Department of Earth Sciences, University of Cambridge, Cambridge CB2 3EQ, UK. Tel.: +44 0 1223333479; Fax: +44 0 1223333450.
E-mail address: giladantler@gmail.com (G. Antler).

http://dx.doi.org/10.1016/j.gca.2017.01.015
0016-7037/

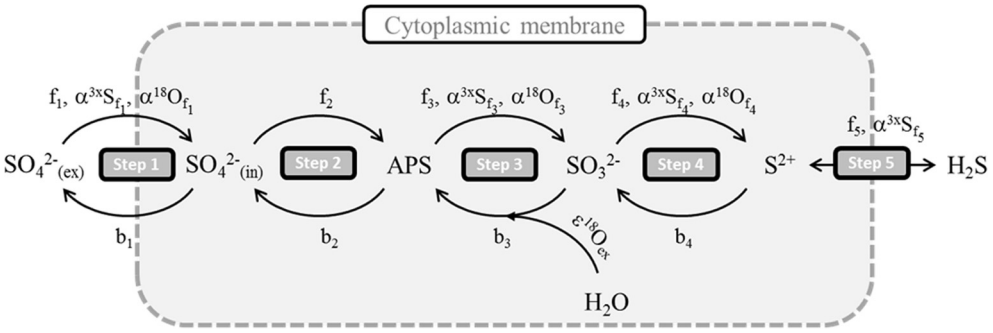

Fig. 1. Schematic of the microbial sulfate reduction pathway. Steps of MSR and the presumed points of oxygen and sulfur isotope fractionation. $i_{\_}j$, $\alpha^{34}S_{i\_j}$ and $\alpha^{18}O_{i\_j}$ are the fluxes and the isotope fractionation factors for sulfur and oxygen, respectively, for the forward ($i = f$) and backward ($i = b$) reactions j ($j = 1\ldots5$). ϕ_k ($k = 1$, 2 and 4) is the ratio between the backward and forward fluxes. $\varepsilon^{18}O_{ex}$ is the fractionation of oxygen isotopes between water and sulfur intermediates.

sulfite and in the absence of the DsrC subunit. Under these conditions, sulfite is reduced to an S^{2+} intermediate, which is then converted to a DsrC trisulfide (Santos et al., 2015). The DsrC trisulfide is then reduced to sulfide by the membrane complex DsrMKJOP (Santos et al., 2015). Because most (if not all) intracellular steps during MSR are reversible, understanding the dynamics among different steps, the controls on their relative reversibilities, and the relationship of these steps with the measurable cell-specific sulfate reduction rate (often abbreviated as csSRR) is critical for understanding the activity and rates of microbial sulfate reduction in nature (Rees, 1973; Farquhar et al., 2003; Brunner and Bernasconi, 2005; Canfield et al., 2006; Eckert et al., 2011; Holler et al., 2011).

The use of isotope geochemistry, specifically the stable sulfur ($^{33}S/^{32}S$ and $^{34}S/^{32}S$) and oxygen ($^{18}O/^{16}O$) isotope ratios (see Appendix 1 for isotope notation), has given insights into the intracellular steps during MSR. Given that every step during MSR partitions each sulfur isotopologue to a different degree and in a different manner, the isotope partitioning of the major or minor sulfur or oxygen isotopes in the extracellular sulfate pool should reflect the relationship between different steps and their reversibilities (assuming the first step is reversible). These are often called 'branching points' which refers to a point in the reaction pathway where isotopic fractionation occurs (e.g., Farquhar et al., 2003). Most studies have employed the ratio of ^{32}S and ^{34}S measured in sulfate, sulfide, or sulfur intermediates to investigate MSR and its branching points (e.g. Canfield, 2001b; Canfield et al., 2006; Canfield et al., 2010; Zerkle et al., 2010; Kamyshny et al., 2011; Knossow et al., 2015). Studies focusing on the fractionation of ^{34}S from ^{32}S during MSR have found that most of the enzymatic steps during MSR prefer the ^{32}S isotope, transferring ^{32}S into the produced sulfide pool and leaving ^{34}S behind in a Rayleigh-type isotope distillation. The magnitude of sulfur isotope fractionation during MSR can be as high as ~70‰ for $\delta^{34}S_{SO4}$ (Wortmann et al., 2001; Canfield et al., 2010; Sim et al., 2011a), and approaches the value expected for sulfur isotopic equilibrium between sulfate and sulfide (71‰ at 25 °C – Tudge and Thode, 1950; Wing and Halevy, 2014).

More recently, studies have employed coupled ^{32}S, ^{33}S, and ^{34}S isotopes (e.g. Farquhar et al., 2003, 2008; Johnston et al., 2005, 2007; Ono et al., 2006; Sim et al., 2011a,b, 2013; Leavitt et al., 2013, 2014, 2015; Pellerin et al., 2015a, b) or $^{34}S/^{32}S$ and $^{18}O/^{16}O$ isotope ratios (Brunner et al., 2005, 2012; Turchyn et al., 2006; Wortmann et al., 2007; Farquhar et al., 2008; Knöller et al., 2006; Gilhooly et al., 2016; Böttcher et al., 1998, 1999, 2006; Mangalo et al., 2007, 2008; Antler et al., 2013, 2014). The coupled isotope approaches are thought to provide information about up to two branching points in the MSR pathway (Fig. 1). During strictly mass-dependent fractionation, the magnitude of $\delta^{33}S_{SO4}$ is about half (0.5147 at 25 °C – Farquhar et al., 2003) that of $\delta^{34}S_{SO4}$. Over the last 60 years, studies have shown that the magnitude of the sulfur isotope fractionation for either $^{34}S/^{32}S$ or $^{33}S/^{32}S$ is a function of microbial metabolism and intracellular pathways which deliver electrons to the sulfate reduction pathway (e.g. Sim et al., 2011b, 2012, 2013; Brüchert, 2004), the amount of sulfate available (e.g. Habicht et al., 2002; Farquhar et al., 2003; Canfield, 2004; Bradley et al., 2016), the temperature (e.g. Canfield et al., 2006; Hoek et al., 2006) and the rate of sulfate reduction (e.g., Chambers et al., 1975; Canfield, 2001a,b; Kaplan and Rittenberg, 1963; Leavitt et al., 2013, 2015; Sim et al., 2011a,b).

The $^{18}O/^{16}O$ ratio in dissolved sulfate ($\delta^{18}O_{SO4}$) also increases as MSR progresses, but often reaches an apparent isotopic equilibrium with water and ceases to increase (Fritz et al., 1989; Böttcher et al., 1998, 1999; Turchyn et al., 2006, 2010; Wortmann et al., 2007; Aller et al., 2010; Zeebe, 2010). Pure culture studies have shown that oxygen atoms from water are incorporated into sulfate during MSR (Mizutani and Rafter 1973; Fritz et al., 1989; Brunner et al., 2005; Mangalo et al., 2007, 2008) much more rapidly than would be expected from the purely abiotic oxygen isotope exchange between water and sulfate under normal surface conditions (pH > 1, temperature < 100 °C) (Lloyd, 1968; Chiba and Sakai 1985; Rennie and Turchyn, 2014). This rapid isotope exchange during MSR is attributed to the intracellular exchange of oxygen atoms between water and sulfur redox intermediate species such as sulfite (Mizutani and Rafter, 1973; Fritz et al., 1989) and occurs

within minutes (Betts and Voss, 1970; Horner and Connick, 2003; Wankel et al., 2014; Müller et al., 2013). If a portion of intracellular sulfite is reoxidized back to sulfate and added to the extracellular sulfate pool, the exchange of oxygen isotopes between sulfite and water will be observed. The observed (and modelled) oxygen isotope enrichment of sulfate relative to the isotopic composition of the water ($\delta^{18}O_{SO4} - \delta^{18}O_{H2O}$) is between 20‰ and 28‰, reflecting this intracellular oxygen isotope exchange and subsequent reoxidation (e.g. Böttcher et al., 1998, 1999; Turchyn et al., 2006, 2010; Wortmann et al., 2007; Zeebe, 2010).

Some experiments with natural populations and observations in the environment show a linear trend between $\delta^{18}O_{SO4}$ and $\delta^{34}S_{SO4}$, demonstrating that both oxygen and sulfur isotopes undergo kinetic isotope fractionation and that the aforementioned isotope equilibrium between sulfate and water is not always observed (e.g. Sivan et al., 2014; Antler et al., 2015). The magnitude of this kinetic isotope fractionation for $\delta^{18}O_{SO4}$ has been suggested to be 25% of the magnitude of $\delta^{34}S_{SO4}$ (Mizutani and Rafter, 1969; Mandernack et al., 2003). Therefore, the oxygen isotope fractionation observed during MSR is thought to result from a combination of the kinetic isotope effect associated with enzymatic steps during MSR (similar to sulfur isotopes), the equilibration of oxygen isotopes between sulfur species in intermediate valence state and water, and the contribution of these sulfur species to the extracellular sulfate pool.

This study aims to: 1. Test whether the major and minor isotopes of sulfur and the oxygen isotope system record complementary information about intracellular processes; and 2. Assess the magnitude of the equilibrium and kinetic oxygen isotope effects. To do this, we experimentally explore the respective evolution of three isotope ratios: $^{33}S/^{32}S$, $^{34}S/^{32}S$ and $^{18}O/^{16}O$ during MSR in pure culture batch experiments as a function of the csSRR and $\delta^{18}O_{H2O}$. These measurements are then used to constrain models of $\delta^{34}S_{SO4}$, $\delta^{33}S_{SO4}$ and $\delta^{18}O_{SO4}$.

2. THE USE OF MODELS OF SULFUR AND OXYGEN ISOTOPE FRACTIONATION DURING MICROBIAL SULFATE REDUCTION

Numerical models of MSR use sulfur ($^{33}S/^{32}S$ and $^{34}S/^{32}S$) and oxygen ($^{18}O/^{16}O$) isotope ratios in dissolved sulfate as experimental constraints, add assumptions about electron flow and maximum isotope fractionations imparted by individual enzymes (Fig. 1), and then solve for the magnitudes of backward and forward fluxes associated with the modelled reactions. These models have been used to reconstruct environmental processes and physiological conditions from observed isotope fractionations (e.g. Farquhar et al., 2003, 2008; Sim et al., 2011b; Brunner et al., 2012). However, the problem is under-constrained, as there are more variables than equations. Many studies work around this limitation by merging several steps together. Most notably, this is done by considering the reduction of sulfite to sulfide in a single step. Brunner et al. (2012) modelled the sulfur and oxygen isotope evolution during MSR, and in doing so determined that a single-step sulfite reduction to sulfide (step 4 and 5— Fig. 1) is not consistent with the isotope data. Combining multiple sulfur and oxygen isotopes should help constrain the problem and provide an equivalent number of variables (the flux ratios at each step—ϕ_i in Fig. 1) and mass balance equation for each isotope ratio. However, only a few studies have combined multiple sulfur and oxygen isotopes (^{32}S, ^{33}S, ^{34}S and ^{18}O and ^{16}O) (e.g. Farquhar et al., 2008). The following section summarizes past modeling efforts for sulfur and oxygen isotopes during MSR.

The overall sulfur isotope fractionation during MSR is modelled as a superposition of the various forward and backward fluxes at each step with any isotope partitioning occurring at each step (Rees, 1973; Farquhar et al., 2003; Brunner and Bernasconi, 2005; Sim et al., 2011b) and is given mathematically by (after Brunner et al. 2012):

$$\alpha^{3x}S_{total} = \frac{\begin{array}{c}\phi_1\cdot\phi_2\cdot\phi_3\cdot\phi_4\cdot(1-\alpha^{3x}S_{f\_5})+\ldots \\ \phi_1\cdot\phi_2\cdot\phi_3\cdot\alpha^{3x}S_{f\_5}\cdot(1-\alpha^{3x}S_{f\_4})+\ldots \\ \phi_1\cdot\phi_2\cdot\alpha^{3x}S_{f\_5}\cdot\alpha^{3x}S_{f\_4}\cdot(1-\alpha^{3x}S_{f\_3})\end{array}}{\alpha^{3x}S_{f\_5}\cdot\alpha^{3x}S_{f\_4}\cdot\alpha^{3x}S_{f\_3}(1)} + 1 \quad (1)$$

where $\alpha^{3x}S_{total}$ is the total expressed sulfur isotope fractionation factor for isotope $3x$ ($x = 3, 4$), $\alpha^{3x}S_{i\_j}$ is the sulfur isotope fractionation during the forward ($i = f$) and backward ($i = b$) reaction j (where $j = 1\ldots5$) and ϕ_k (where $k = 1\ldots4$) is the ratio between the fluxes of the four intracellular steps summarized in Fig. 1:

$$\phi_k = \frac{b_k}{f_k} \quad (2)$$

Thus, models of MSR (Rees, 1973; Farquhar et al., 2003; Brunner and Bernasconi, 2005; Johnston et al., 2007; Sim et al., 2011b; Brunner et al., 2012) assign values for sulfur isotope fractionation factors in the forward steps 1, 3, 4 and 5, respectively, and assume that all other steps (and backward reactions) do not fractionate sulfur isotopes – e.g., Rees (1973). Because the isotopic fractionation at step 1 is very small, and there is no fractionation in step 3, all solutions are virtually symmetrical for both of these steps. Therefore, using isotopic techniques, it is impossible to distinguish one from the other.

For minor isotopes (such as ^{33}S), the relationship between the isotope fractionation for $^{33}S/^{32}S$ (compared with $^{34}S/^{32}S$) is commonly given as (e.g. Harrison and Thode, 1958; Young et al., 2002; Farquhar et al., 2003)

$$\ln(\alpha^{33}S) = \vartheta^* \cdot \ln(\alpha^{34}S) \quad (3)$$

where ϑ^* is the calculated temperature-dependent equilibrium isotope fractionation between sulfate and sulfide (0.5147 – Farquhar et al., 2003). The deviation between the calculated value for $\alpha^{33}S$ and the expected mass-dependent relationship between $\alpha^{33}S$ and $\alpha^{34}S$ is defined as:

$$E^{33}S = 1000 \cdot \left(\alpha^{33}S - \alpha^{34}S^{0.515}\right) \quad (4)$$

The partitioning of ^{33}S in every step during MSR does not deviate from a mass-dependent fractionation with respect to ^{34}S (Eq. (2)), but the overall expressed isotope fractionation can deviate from a purely mass-dependent

relationship. The magnitude of this offset is a function of the relative forward and backward fluxes of every step during MSR and stems from the fact that the mixing between two pools is linear, but the mass-dependent fractionation obeys a power law (Farquhar et al., 2003, 2007; Ono et al., 2006; Johnston et al., 2007). Mixing between two pools with variable branching points is common in metabolisms such as MSR, and it has been used in the past to calculate the dynamics of the forward and backward fluxes of each step during MSR (e.g., Farquhar et al., 2003; Sim et al., 2011b; Johnston et al., 2007). Fig. 2a shows an example of these calculations.

Oxygen isotopes in dissolved sulfate ($\delta^{18}O_{SO4}$ values) are thought to record information complementary to that revealed by sulfur isotopes. The relative change between $\delta^{18}O_{SO4}$ and $\delta^{34}S_{SO4}$ has been used as a tracer of pyrite oxidation (e.g. Balci et al., 2007; Brunner et al., 2008; Heidel and Tichomirowa, 2011; Kohl and Bao, 2011), sulfur disproportionation (e.g. Cypionka et al., 1998; Böttcher et al., 2001; Böttcher and Thamdrup, 2001; Böttcher et al., 2005; Poser et al., 2016), cryptic cycling of sulfur (e.g., Mikucki et al., 2009; Aller et al., 2010; Riedinger et al., 2010; Johnston et al., 2014) and sulfate-driven anaerobic oxidation of methane (e.g. Avrahamov et al., 2014; Aharon and Fu, 2000, 2003; Antler et al., 2014, 2015; Deusner et al., 2014; Sivan et al., 2014). Changes in the reversibility of all steps during MSR (Fig. 1) change the composition of oxygen and sulfur isotopes of extracellular sulfate as MSR progresses. This is expressed mathematically as (after Brunner et al., 2012; Antler et al., 2013):

$$\delta^{18}O_{SO4(t)} = \begin{cases} \frac{\varepsilon^{18}O_{total}}{\varepsilon^{34}S_{total}} \cdot \left(\delta^{34}S_{SO4(t)} - \delta^{34}S_{SO4(0)}\right) + \delta^{18}O_{SO4(0)} & \phi_1 \cdot \phi_2 \cdot \phi_3 = 0 \\ \delta^{18}O_{SO4(A.E)} - exp\left(-\theta_O \cdot \frac{\delta^{34}S_{SO4(t)} - \delta^{34}S_{SO4(0)}}{\varepsilon^{34}S_{Stotal}}\right) \ldots \\ \quad \cdot\left(\delta^{18}O_{SO4(A.E)} - \delta^{18}O_{SO4(0)}\right) & 0 < \phi_1 \cdot \phi_2 \cdot \phi_3 < 1 \end{cases} \quad (5)$$

where $\varepsilon^{34}S_{total}$ and $\varepsilon^{18}O_{total}$ are the measured sulfur and oxygen isotope fractionation, respectively, and $\delta^{34}S_{SO4(t)}$, $\delta^{34}S_{SO4(0)}$, $\delta^{18}O_{SO4(t)}$ and $\delta^{18}O_{SO4(0)}$ are the isotopic compositions of sulfur and oxygen in the residual sulfate at time t and time 0, respectively. $\delta^{18}O_{SO4(A.E)}$ is the isotopic composition of oxygen in the residual sulfate at apparent equilibrium, and θ_O is a parameter initially formulated by Brunner et al. (2005). This parameter measures the ratio between the apparent oxygen isotope exchange and sulfate reduction rate (Brunner et al., 2012):

$$\theta_O = \frac{\phi_1 \cdot \phi_2 \cdot \phi_3}{1 - \phi_1 \cdot \phi_2 \cdot \phi_3} \quad (6)$$

Factorization of Eq. (5) suggests that there are two distinct stages on a cross-plot of $\delta^{18}O_{SO4}$ vs. $\delta^{34}S_{SO4}$ during bacterial sulfate reduction:

(1) Apparent linear phase: The initial segment of the $\delta^{18}O_{SO4}$ vs. $\delta^{34}S_{SO4}$ cross-plot during MSR can be approximated by a linear line. The mathematical term for this line can be described by the first term of the Taylor series of Eq. (5) around $\delta^{34}S_{SO4(0)}$ and $\delta^{18}O_{SO4(0)}$ (Antler et al., 2013). The slope of this apparent linear (SALP) phase can therefore be written as:

$$SALP = \theta_O \frac{\delta^{18}O_{SO4(A.E)} - \delta^{18}O_{SO4(0)}}{\varepsilon^{34}S_{total}} \quad (7)$$

The value of the SALP can vary between 0.25 to over 10 and depends on the sulfate reduction rate (Böttcher et al., 1998, 1999; Aharon and Fu, 2000; Brunner et al., 2006; Antler et al., 2013) and the type and supply rate of the electron donor (Antler et al., 2014; Antler et al., 2015).

(2) Apparent equilibrium phase: This is the last segment on the $\delta^{18}O_{SO4}$ vs. $\delta^{34}S_{SO4}$ cross plot, where the $\delta^{18}O_{SO4}$ reaches a constant value while the $\delta^{34}S_{SO4}$ continues to increase. In the natural environment, the $\delta^{18}O_{SO4}$ equilibrium value has been observed to be between 22‰ and 28‰ larger than the $\delta^{18}O$ value of the water (e.g. Knöller

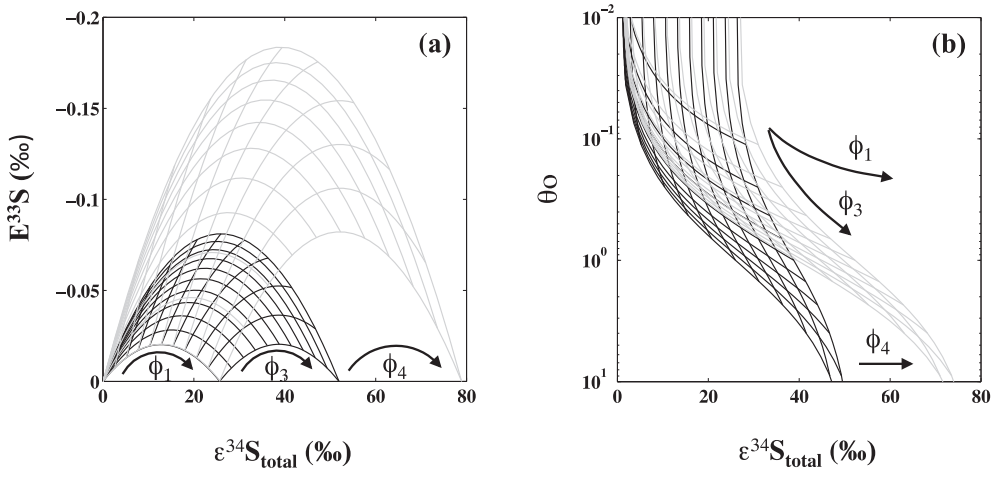

Fig. 2. Model predictions of flux ratios that produce different $E^{33}S$, $\varepsilon^{34}S_{total}$ and θ_O values. (a) $E^{33}S$ vs. $\varepsilon^{34}S_{total}$ diagram. (b) θ_O vs. $\varepsilon^{34}S_{total}$ diagram. The black and the gray meshes, respectively, in both panels are the solutions where ϕ_4 (the ratio of fluxes in step 4, the reduction of sulfite to S^{2+}—Fig. 1) is minimal (=0) and maximal (=1), respectively. The arrows show the direction by which each flux ratio (Fig. 1) changes in the diagrams. According to numerical models, if two of the three values of $E^{33}S$, $\varepsilon^{34}S_{total}$, and θ_O are measured, the result will plot within the black and the grey meshes and enables solving for the relative fluxes at two steps during MSR. Here, we assume isotope fractionations at steps 3, 4 and 5 to be $\alpha^{34}S = 0.975$ (Brunner et al., 2012) and $\vartheta^* = 0.5147$ (Farquhar et al., 2003).

et al., 2006; Turchyn et al., 2006; Wortmann et al., 2007). This large range of oxygen isotope equilibrium values may reflect isotope exchange at different temperatures (Fritz et al., 1989; Zeebe, 2010) or reflect the combined effect of kinetic and equilibrium oxygen isotope fractionations (Wortmann et al., 2007; Turchyn et al., 2010). The latter is named apparent equilibrium ($\delta^{18}O_{SO4(A.E)}$). Several sulfur intermediates have been suggested to exchange oxygen isotopes with water; most notably APS (e.g. Mizutani and Rafter, 1973; Fritz et al., 1989), sulfite (e.g. Müller et al., 2013; Wankel et al., 2014) and when sulfite is bound to adenosine mono-phosphate (e.g. Wortmann et al., 2007; Wankel et al., 2014). Recent studies have ruled out the equilibrium between APS and water (Brunner et al., 2012; Kohl et al., 2012). Under cytoplasmic pH (6–7), sulfite reaches isotopic equilibration in matters of minutes (Betts and Voss, 1970; Wankel et al., 2014); the rapidity of the oxygen isotope equilibrium implies that sulfite in the cell is fully equilibrated with water. The value of apparent equilibrium, including the effect of the kinetic oxygen isotope fractionation, is expressed mathematically as:

$$\delta^{18}O_{SO4(A.E)} = \delta^{18}O_{H2O} + \varepsilon^{18}O_{ex} + \frac{\varepsilon^{18}O_{f\_1}}{\phi_1 \cdot \phi_2 \cdot \phi_3} + \frac{\varepsilon^{18}O_{f\_3}}{\phi_3} \quad (8)$$

A useful way to study the mutual evolution of $\delta^{18}O_{SO4}$ and $\delta^{34}S_{SO4}$ with respect to the progress of MSR (e.g. the decrease in sulfate concentration with time during MSR) is to plot θ_O vs. $\varepsilon^{34}S_{total}$ (Fig. 2b). Previous studies have used this cross-plot to investigate the mechanism of MSR (Brunner et al., 2005, 2012; Knöller et al., 2006; Turchyn et al., 2010; Antler et al., 2013) and sulfate-driven anaerobic methane oxidation (Deusner et al., 2014). Because both $\varepsilon^{34}S_{total}$ and θ_O are functions of the forward and backward fluxes during MSR (Eqs. (1) and (6), respectively), this plot can be used to relate sulfur and oxygen isotope measurements to the intracellular MSR fluxes. This is because for every set of given forward and backward fluxes, there are specific values of θ_O and $\varepsilon^{34}S_{total}$. However, because there are more branching points in the framework of MSR than the solution for θ_O and $\varepsilon^{34}S_{total}$, the ratio of between the forward and backward fluxes of every branching point cannot be solved uniquely. Fig. 2b also demonstrates the relationship between θ_O vs. $\varepsilon^{34}S_{total}$ and the ratio of intracellular fluxes.

The plot of θ_O vs. $\varepsilon^{34}S_{total}$ (Fig. 2b) has similarities to the plot of $E^{33}S$ vs. $\varepsilon^{34}S_{total}$ (Fig. 2a), but typically only one of these two is used. The central question asked by this study is whether the use of combined θ_O vs. $\varepsilon^{34}S_{total}$ and $E^{33}S$ vs. $\varepsilon^{34}S_{total}$ diagrams can enable the probing of different processes and reaction rates during MSR. We hypothesize that this combined isotope approach can explore a wider range of steps in the modeled MSR network, not all of which may be inferred by using θ_O vs. $\varepsilon^{34}S_{total}$ or $E^{33}S$ vs. $\varepsilon^{34}S_{total}$ plots alone.

3. METHODS

Pure cultures of marine sulfate reducing bacterium *Desulfovibrio* sp. (strain DMSS-1—Sim et al., 2011b) were incubated in batch at room temperature (22 °C) in the dark (see Sim et al., 2011b for the medium recipe). DMSS-1 was grown on five different organic substrates (lactate, malate, ethanol, fructose and glucose at limiting concentrations) that served as both the electron donors and carbon sources. Each incubation experiment with different organic substrates was repeated three times using isotopically enriched water with different initial oxygen isotope compositions (Table 1). The use of ^{18}O-enriched water serves a way to enhance the signal of the measured $\delta^{18}O_{SO4}$. Furthermore, by comparing the change in $\delta^{18}O_{SO4}$ from experiments using different $\delta^{18}O_{H2O}$ we can distinguish the contribution of oxygen exchange with water from other isotopic effects (such as kinetic isotope fractionation).

The Achilles' heel of batch culture experiments is that the system is not in steady state. This might have a significant influence on evolution of $\delta^{18}O_{SO4}$ and $\delta^{34}S_{SO4}$. Nevertheless, Sim et al. (2011b) performed experiments under similar conditions (using the same strain and the same electron donors) in both batch and flow-through reactors and found that there were no significant differences between the expressed sulfur fractionation between the two. Small changes between the two conditions are still possible, but would not be detected by the experimental design in our studies or any comparable studies.

Bacteria were pre-cultured on the respective electron donors before inoculation: about 1 ml of preculture was spun down anaerobically, the pellet was washed with fresh medium three times to remove sulfide and then transferred to 100 ml of fresh medium. Then, this medium was transferred in 10-ml aliquots to seven or eight 15 ml vials. Each of the vials was sacrificed at different time points during the experiment by removing 1 ml for cell counts and sulfide measurements and injecting 2 ml of 20% Zn acetate to precipitate zinc sulfide. Most of this solution was used to measure multiple sulfur isotopes. Two milliliters of the Zn-treated culture were filtered. Half of the filtrate was used to measure the sulfate concentration and the other half was mixed with 1 ml of the saturated BaCl solution to precipitate barite ($BaSO_4$).

3.1. Analytical methods

Sulfate concentrations were measured by ion chromatography (IC, Dionex DX5000) with an error of 3% between duplicates. Sulfide concentrations were measured by spectrophotometer using a modified methylene blue assay (Cline, 1969). Cell density was measured by epifluorescence microscopic counts of cells stained by SYTOX®

Table 1
Combinations of electron donors (rows) and isotopic composition of the water ($\delta^{18}O_{H2O}$ – columns) used in experiments. '+' marks the explored combination.

	−5‰	35‰	75‰
Lactate	+	+	+
Malate	+		+
Ethanol	+	+	+
Fructose	+	+	+
Glucose	+	+	+

Green nucleic acid stain (Life Technologies, Grand Island, NY, USA).

For the analysis of $\delta^{18}O_{SO4}$, barite was pyrolyzed at 1450 °C in a temperature conversion element analyzer (TC/EA), producing carbon monoxide. Carbon monoxide was measured by continuous helium flow in a GS-IRMS (Thermo Finnegan Delta V Plus, at the Godwin Laboratory, University of Cambridge). To analyse the $\delta^{34}S_{SO4}$, barite was combusted at 1030 °C in a flash element analyzer (EA), and the resulting sulfur dioxide (SO_2) was measured by continuous helium flow on a GS-IRMS (Thermo Finnegan Delta V Plus Godwin Laboratory, University of Cambridge). Analyses of $\delta^{18}O_{SO4}$ were conducted in replicates ($n = 3$–5) and the standard deviation was determined using the standard NBS 127 (~0.3‰ 1σ). The error for $\delta^{34}S_{SO4}$ was determined using the standard deviation of standards run at the beginning and the end of each run (~0.3‰ 1σ). Measurements of $\delta^{18}O_{SO4}$ and $\delta^{34}S_{SO4}$ were corrected to NBS 127 and IAEA-SO-6 ($\delta^{18}O_{SO4}$ of 8.6‰, −11.35‰ and $\delta^{34}S_{SO4}$ of 20.3‰, −34.1‰, respectively). $\delta^{34}S_{SO4}$ is reported with respect to Vienna Canyon Diablo Troilite (VCDT) and $\delta^{18}O_{SO4}$ is reported relative to the Vienna Standard Mean Ocean Water (VSMOW). Appendix 3 discusses the validation of measurements of exceptionally high $\delta^{18}O_{SO4}$.

To conduct multiple sulfur isotope measurements ($\delta^{33}S$ and $\delta^{34}S$), Ag_2S samples were reacted with an excess of fluorine gas at 300 °C, following the procedure described in Ono et al. (2006). This produced SF_6 gas, which was purified by gas chromatography and transferred into Thermo Finnegan MAT 253 for multiple sulfur isotope measurements. Sulfide generated during growth was extracted by acidifying the zinc sulfide precipitate with 6 N HCl at 80 °C under nitrogen gas for two hours. H_2S(g) produced during this distillation was re-precipitated as zinc sulfide in a zinc–acetate solution (0.18 M). After the extraction of sulfide, the samples were purged by nitrogen gas for an additional hour to ensure the complete removal of sulfide. Sulfate in the remaining medium was reduced to sulfide by reacting with 30 ml of the reducing agent (mixture of HI, H_3PO_2 and HCl, Thode et al., 1961). The samples were boiled and purged by N_2 gas. The volatile products were passed through a condenser and a trap containing distilled water and sulfide gas generated by sulfate reduction was collected in the zinc–acetate trap. The analytical reproducibility of measurements using the fluorination method, as determined by repeated analyses of international reference material, is ±0.1‰ and ±0.2‰ for $\delta^{33}S$ and $\delta^{34}S$, respectively.

$\delta^{18}O_{H2O}$ was measured by a Continuous Flow Gas Source Isotopic Ratio Mass Spectrometer (CF-GS-IRMS Thermo, at the Godwin Laboratory, University of Cambridge) coupled to a Gas Bench II (GBII) interface. Vials containing 0.5 ml of the sample were flushed with helium and 0.4% CO_2 gas-mixture and the samples were measured after equilibrating with the gas mixture for 24 h. Samples were corrected to three standards (−7.3, 0.2 and 11.2‰). The error of the measurement was ±0.1‰. $\delta^{18}O_{H2O}$ reported versus Vienna Standard mean Ocean water (VSMOW).

4. RESULTS

All results are tabulated in the supporting online material. DMSS-1 grew and reduced sulfate under all tested conditions. Fig. 3 is a composite figure showing sulfate concentrations and $\delta^{34}S_{SO4}$ and $\delta^{18}O_{SO4}$ measured in experiments with all different electron donors in experiments with the $\delta^{18}O_{H2O}$ of 72 ± 1‰. The results of the cultures grown in water with different $\delta^{18}O_{H2O}$ show very similar trends and are presented in the Supplementary material. Sulfate concentrations decreased with time, as expected during MSR. Cell densities, and $\delta^{34}S_{SO4}$ and $\delta^{18}O_{SO4}$ increased with time in all experiments. The largest and the smallest decrease in sulfate concentration were observed in the experiments with lactate and glucose, respectively. The $\delta^{34}S_{SO4}$ and $\delta^{18}O_{SO4}$ showed the opposite trend, where sulfur and oxygen isotope ratios changed faster when DMSS-1 grew on glucose than when the bacterium grew on lactate (Fig. 3).

To compare sulfur isotope enrichments among the experiments, we plot the change in $\delta^{34}S_{SO4}$ from its initial value ($\delta^{34}S_{SO4}(t) - \delta^{34}S_{SO4}(0)$) against the natural logarithm of the ratio of the remaining sulfate (Fig. 4a); The more rapidly the $\delta^{34}S_{SO4}$ changes with the decreasing sulfate concentration, the bigger the sulfur isotope enrichment or fractionation. The growth on glucose resulted in the highest sulfur isotope fractionation. Decreasing sulfur isotope fractionation occurred in cultures grown on fructose, malate, ethanol and lactate. The cross-plot of $\delta^{18}O_{SO4}$ vs. $\delta^{34}S_{SO4}$ (Fig. 4b) demonstrates the relative changes of the $\delta^{18}O_{SO4}$ and $\delta^{34}S_{SO4}$ in different experiments. The $\delta^{18}O_{SO4}$ exhibited the largest and smallest changes, respectively, relative to the changes in $\delta^{34}S_{SO4}$ during growth on glucose and lactate, respectively.

5. DISCUSSION

5.1. Placing a limit on kinetic oxygen isotope fractionation

Studies on MSR use $\delta^{18}O_{SO4}$ mainly to target the reoxidation of intracellular reduced sulfur species, although the potential importance of kinetic oxygen isotope fractionation is becoming increasingly recognized (Brunner et al., 2005, 2012; Turchyn et al., 2006; Wortmann et al., 2007; Farquhar et al., 2008; Aller et al., 2010, 2013; Wankel et al., 2014), because it can influence the $\delta^{18}O_{SO4}$ at 'apparent equilibrium' (Wortmann et al., 2007; Turchyn et al., 2010; Antler et al., 2013—see also Eq. (8)). Some studies assume that kinetic oxygen isotopic fractionation does not occur (Brunner et al., 2005, 2012), and some estimate an overall kinetic oxygen isotope fractionation as high as 10‰ during MSR (Wankel et al., 2014). Turchyn et al. (2010) suggested that the kinetic oxygen isotope fractionation could not exceed 4‰. All these assumptions lead to differing conclusions about cellular fluxes of sulfur and electrons during MSR and complicate interpretations of environmental data.

Kinetic fractionation of oxygen isotopes can only be studied when the effect of water-isotope equilibrium on the $\delta^{18}O_{SO4}$ is minimal. This is only valid as we assume that

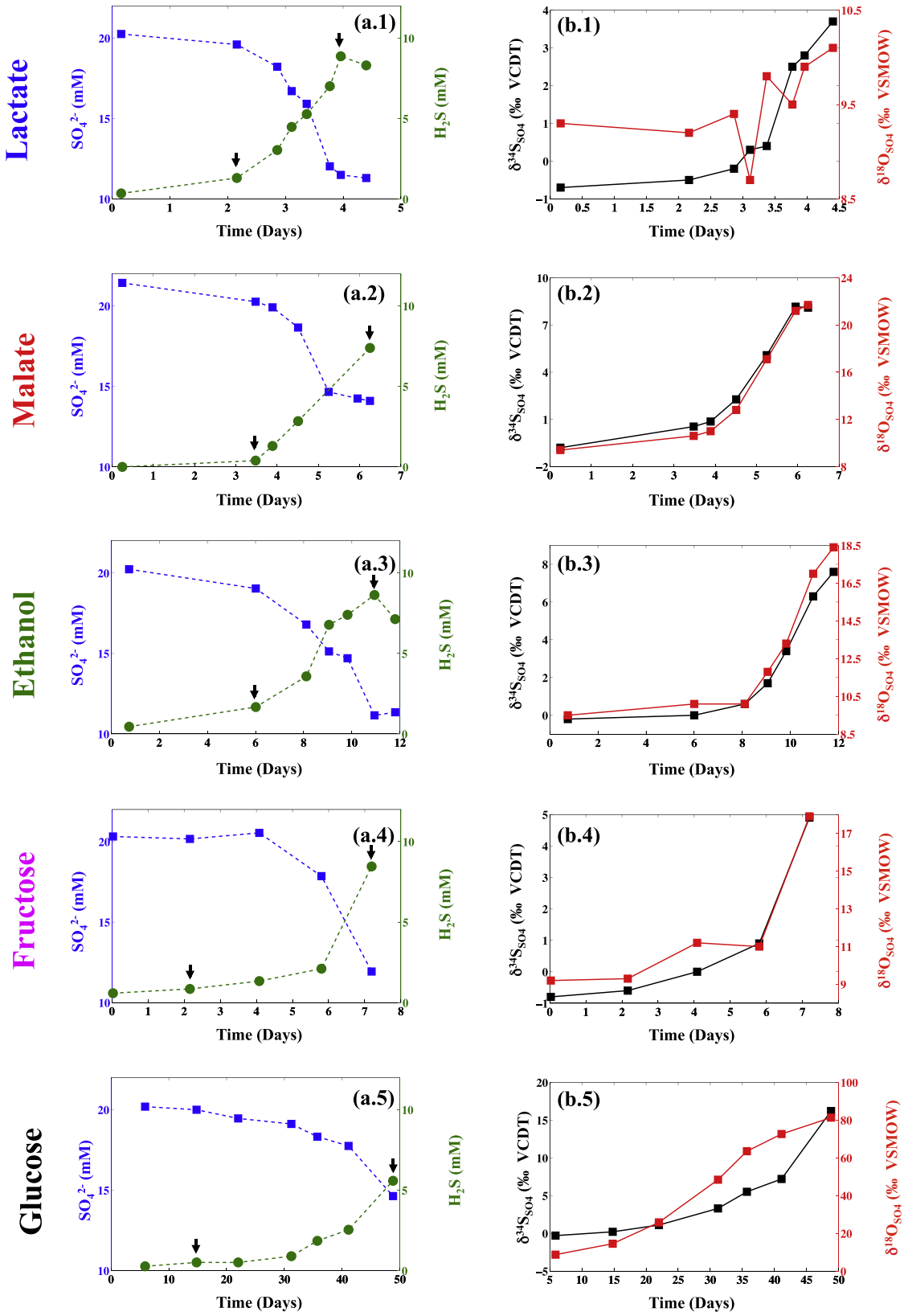

Fig. 3. Sulfate (SO_4^{2-}) and sulfide (H_2S) concentrations (a) and $\delta^{34}S_{SO4}$ and $\delta^{18}O_{SO4}$ values (b) in DMSS-1 cultures grown on lactate (#.1), malate (#.2), ethanol (#.3), fructose (#.4) and glucose (#.5) (where # indicates panels a and b). In all cultures, $\delta^{18}O_{H2O} = \sim 75‰$. Results for other examined $\delta^{18}O_{H2O}$ can be found in Table S1 in the supplemental online material. The arrows indicate the range where csSRR was calculated from.

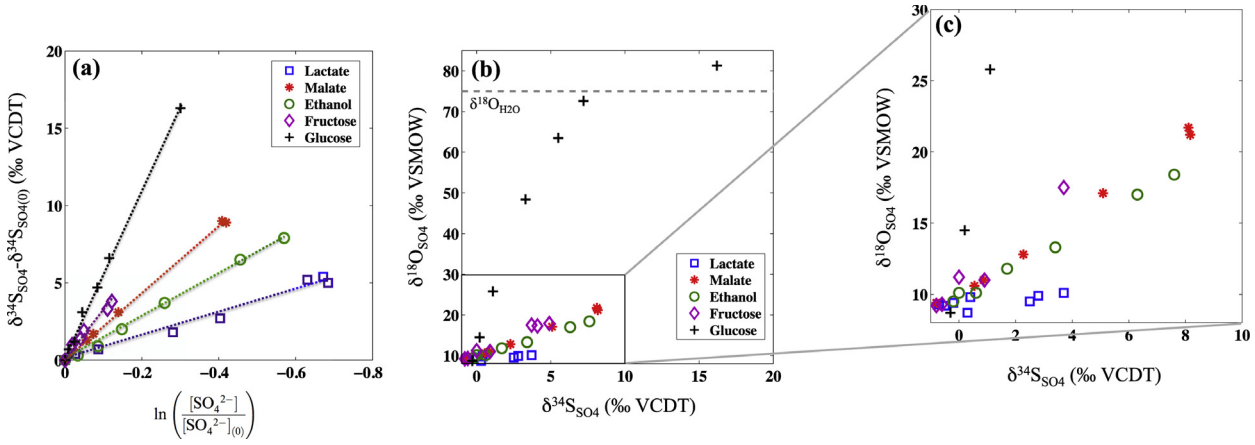

Fig. 4. Enrichments of oxygen and sulfur isotopes in sulfate. Sulfur isotope ratios vs. the natural logarithm of the residual sulfate fraction left in the experiment after bacterial sulfate reduction (a), $\delta^{18}O_{SO4}$ vs. $\delta^{34}S_{SO4}$ (b). The rightmost panel shows an enlargement of the middle panel (c).

the exchange between water (minutes in intracellular pH of 6–7—Wankel et al., 2014) is longer than the residence time of sulfite in the cell. We explore this by plotting the slope of the apparent linear phase ('SALP', Section 2, Eq. (7)) against the oxygen isotope composition of water for all our studied cultures (Fig. 5a). Our experiments demonstrate that the oxygen isotopic composition of water affects the calculated SALP in all experiments, including conditions that previously would have been interpreted as primarily kinetically driven. Therefore, an equilibrium component contributes to the total oxygen isotope fractionation between sulfate and water under all tested conditions.

The experiment exhibiting the smallest influence of the oxygen isotope equilibrium can place an upper limit on the potential magnitude of the total kinetic oxygen isotope fractionation. Fig. 5a shows that the kinetic isotope effect has the largest contribution to the measured $\delta^{18}O_{SO4}$ in cultures grown on lactate. This experiment, grown in water with a $\delta^{18}O_{H2O}$ of −5.3‰, yielded the smallest calculated slope of the apparent linear phase (SALP, Fig. 3). This slope, 0.009 ± 0.03, suggests that the kinetic isotope fractionation of oxygen isotopes relative to the fractionation of sulfur isotopes is negligible at high cell specific sulfate reduction rates. However, the variation in $\delta^{18}O_{SO4}$ in the lactate experiment is very small (~1‰) and the error of the analytical measurement of $\delta^{18}O_{SO4}$ values is high (about 0.4‰), requiring a more conservative calculation. Therefore, we consider the experiment with malate, which exhibited the second smallest experimental slope (Malate-Fig. 5a). In this case, the slope was still smaller than 0.25, which suggests that the magnitude of the kinetic oxygen isotope fractionation cannot be larger than 25% of the magnitude of the kinetic isotope fractionation for sulfur isotopes. Overall, we suggest that the kinetic oxygen isotope fractionation ($\varepsilon^{18}O_{total}$) is between 0‰ and 5‰ (between 0% and 25% of the kinetic sulfur isotope fractionation $\varepsilon^{34}S_{total}$ – 20‰ for the experiment with malate). This value is in agreement with Brunner et al. (2005, 2012) and estimates derived by Turchyn et al. (2010) in pure culture studies, but different from some environmental studies of sites

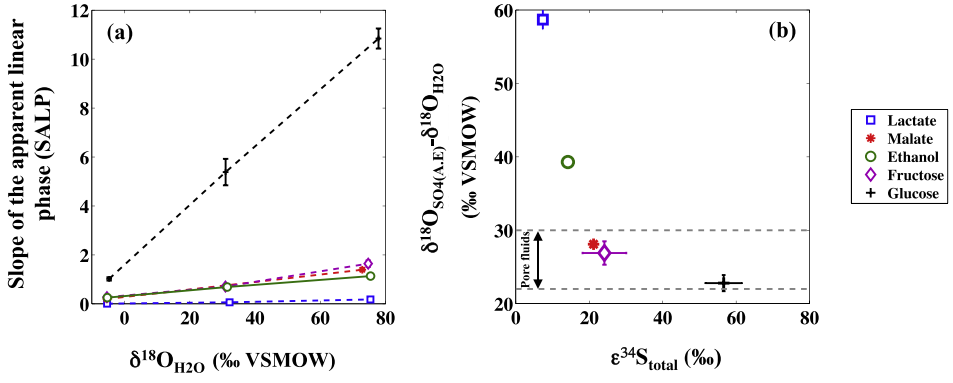

Fig. 5. The slope of the apparent linear phase on the $\delta^{18}O_{SO4}$ vs. $\delta^{34}S_{SO4}$ cross-plot (SALP) plotted against the oxygen isotopic composition of water used in the experiments (a). The apparent equilibrium value of $\delta^{18}O_{SO4}$ ($\delta^{18}O_{SO4(A.E)}$- $\delta^{18}O_{H2O}$) in each experiment plotted against the sulfur isotopic fractionation $\varepsilon^{34}S_{total}$ in each experiment (b). The dashed lines represent the rang of $\delta^{18}O_{SO4(A.E)}$- $\delta^{18}O_{H2O}$ from pore fluids sulfate.

where methane is highly abundant and sulfate reduction rate are high, and linear correlations on the $\delta^{18}O_{SO4}$ vs. $\delta^{34}S_{SO4}$ cross-plot have slopes between 0.34 and 0.5 (Sivan et al., 2014; Antler et al., 2015). These observations indicate that: 1. MSR in nature can be associated with kinetic oxygen isotope fractionations larger than 5‰ at high rates of sulfate reduction or 2. processes other than MSR control the observed oxygen isotope fractionation.

The calculated $\delta^{18}O_{SO4(A.E)}$ (Fig. A.4, Appendix 2) for each of our experiments are presented in Fig. 5b as a function of the csSRR. There is an inverse correlation between the $\delta^{18}O_{SO4(A.E)}$ and the csSRR. Because our experiments were conducted at the same temperature (~22 °C) and at the same time, we can rule out temperature effects on these different isotope equilibria. Instead, factors related to cell physiology and growth conditions are likely to modify the value of $\delta^{18}O_{SO4(A.E)}$. This correlation validates the idea that MSR can generate a range of apparent equilibrium values, rather than a fixed value (Wortmann et al., 2007; Turchyn et al., 2010; Wankel et al., 2014; Antler et al., 2013). This correlation also demonstrates that the kinetic oxygen isotope fractionation impacts the $\delta^{18}O_{SO4}$ much more than the equilibrium fractionation under growth conditions that favour high csSRRs. Eq. (8) predicts this, because at high csSRRs, the uptake of sulfate and its reduction to sulfite are not reversible and the $\delta^{18}O_{SO4}$ at equilibrium approaches infinity.

5.2. Tracing of intracellular sulfur metabolism during microbial sulfate reduction

The sulfur isotope fractionation factor in our experiments was calculated using Rayleigh-type distillation by plotting the change in the isotopic composition of sulfur against the natural log of the fraction of the remaining sulfate (Fig. 4a). Typically, studies report an inverse correlation between $\varepsilon^{34}S_{total}$ and the sulfate reduction rate (e.g. Chambers et al., 1975; Canfield, 2001a,b; Sim et al., 2011a,b; Leavitt et al., 2013, 2015; Ono et al., 2014). Our experiments used different organic donors to change the csSRR and reproduced the same inverse relationship between the csSRR and the magnitude of sulfur isotope fractionation (Fig. 6a). This is consistent with previous culture studies of DMSS-1 (Sim et al., 2011a,b). Models attribute small overall sulfur isotope fractionations to the lower fluxes of intracellular sulfur intermediates that are being oxidized back to the sulfate pool (e.g. Rees, 1973; Farquhar et al., 2003; Brunner and Bernasconi, 2005; Canfield et al., 2006; Wing and Halevy, 2014).

Minor sulfur isotopes ($^{34}S/^{32}S$ and $^{33}S/^{32}S$) provide information about the mixing among different pools of metabolites during MSR (see Fig. 2a). Fig. 6b plots the $E^{33}S$ and $\varepsilon^{34}S_{total}$ values calculated from our experimental results. Our results fall within the grey mesh of model space for $\phi_4 = 1$ (the flux ratio of step 4 – the reduction of sulfite to polysulfide – Fig. 1). However, the plot of our data together with previously published data using the same strain and electron donors (DMSS-1 – Sim et al., 2011a, b) shows that the $E^{33}S$ vs. $\varepsilon^{34}S_{total}$ data cannot be explain solely by assuming $\phi_4 = 1$ or $\phi_4 = 0$ (since not all data fall within the envelopes for the two end member solutions: $\phi_4 = 0$ and $\phi_4 = 1$) and that additional information is needed to solve the intracellular fluxes uniquely.

Changes in the oxygen isotope composition of sulfate can provide some additional information about MSR. Fig. 6c shows θ_O calculated from the data obtained in the five different electron donor experiments (see Eq. (A.5), Appendix 2) plotted against $\varepsilon^{34}S_{total}$ (similar to Fig. 2b). The larger θ_O are associated with the larger $\varepsilon^{34}S_{total}$. Notably, not all the data fall within the envelopes for the two end member solutions ($\phi_4 = 0$ and $\phi_4 = 1$, black lines and grey lines, respectively, Fig. 6c). The presence of some data points outside the modelled space in $E^{33}S$ vs. $\varepsilon^{34}S$ and θ_O vs. $\varepsilon^{34}S_{total}$ plots (Fig. 6a–c) is consistent with observations made by Sim et al. (2011b) and Brunner et al. (2012). In practice, this indicates that previous models that account for two branching points during MSR, as constrained by stable isotopes of sulfur and csSRRs, do not adequately explain all observations that have been made in pure culture and in the natural environment. Therefore, our model considered three branching points instead of two, which is in line with recent revision of the sulfate reduction pathway (Santos et al., 2015). The sulfur isotope fractionation was taken as $\alpha^{34}S = 0.975$ at each of the commonly-used branching points (e.g. Brunner et al., 2012).

Our experiments with DMSS-1 grown on different electron donors probe csSRRs that vary over two orders of magnitude. The increase in csSRR and the accompanying variations in the stable sulfur ($^{33}S/^{32}S$ and $^{34}S/^{32}S$) and oxygen ($^{18}O/^{16}O$) isotope ratios can be used to further explore the dynamics of MSR and solve uniquely the fluxes at three branching points within the cells. This flux ratio solution (ϕ_1,ϕ_3 and ϕ_4) is shown in Fig. 6d as a function of the csSRR; the ratios of fluxes at all assumed branching points are inversely correlated with the csSRR.

Oliveira et al. (2008) suggested that a subunit of dissimilatory sulfite reductase, DsrC, plays a key role in the reduction of S^0 produced by DsrAB. More recently it was confirmed that the csSRR is indeed determined at the cellular level by the DsrC subunit (Santos et al., 2015). Our calculations (Fig. 6d) show that: (1) fluxes at all three modelled branching points exhibit an inverse correlation with the overall csSRR with similar slopes between the ratios of fluxes and csSRR and (2) the first four branching points or steps do not appear to limit the overall MSR process. Given our model assumption that the MSR machinery consists of three branching points, we therefore suggest that the csSRR directly influences the reversibility at all branching points under our experimental conditions. This implies that the last step (step 5, the reduction of S^{2+} to sulfide—Fig. 1) is the rate-limiting step. Our results therefore, are consistent with the observation made by Santos et al. (2015). We suggest the availability of the organic matter, and therefore electrons, controls the availability of the DsrC subunit which is directly linked to the expression of sulfur and oxygen isotope fractionation during MSR.

5.3. Environmental implications

To what extent do results from pure culture experiments such as ours explain the geochemical variability in the

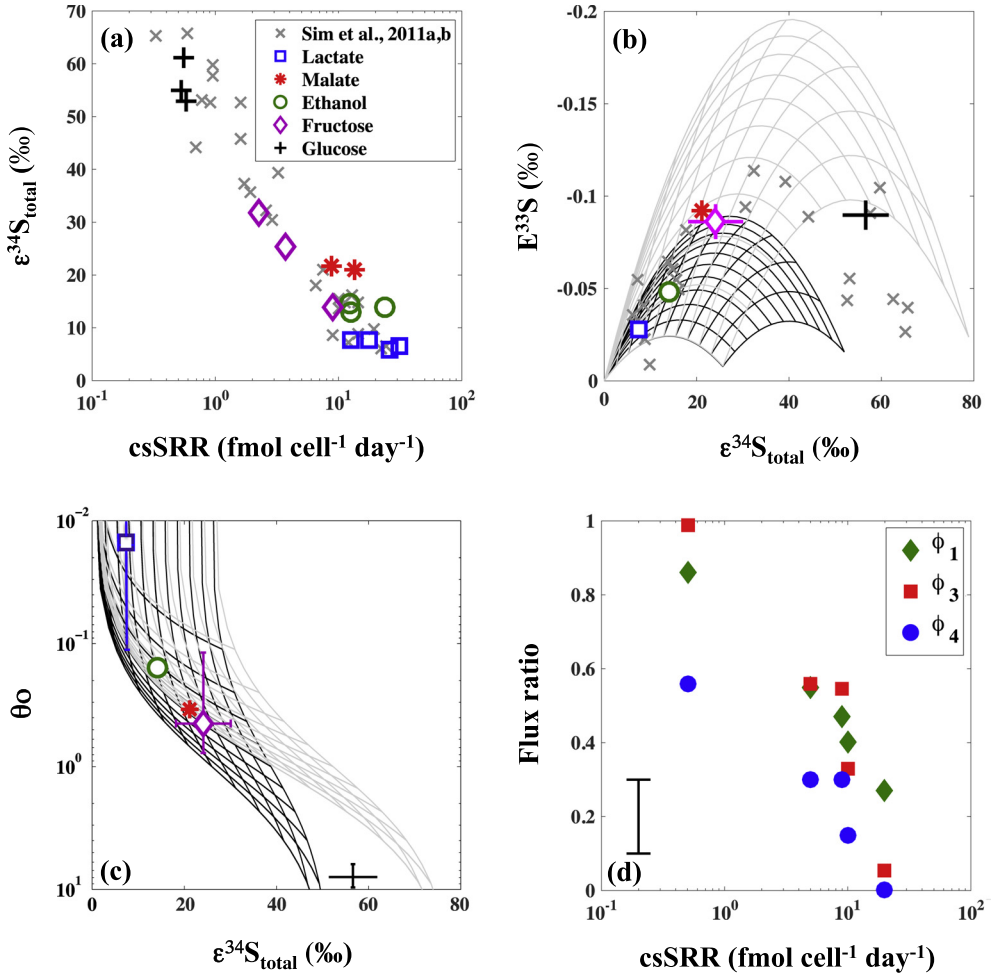

Fig. 6. Isotopic fractionation. (a) Fractionation of $^{34}S/^{32}S$ as a function of the cell specific sulfate reduction rate in this study. Data from Sim et al. (2011a,b) are plotted for comparison. $\varepsilon^{33}S$ vs. $\varepsilon^{34}S_{total}$ (b) and the θ_O vs. $\varepsilon^{34}S_{total}$ (c) diagram; the black and the gray meshes, respectively, in both panels are the solutions where ϕ_4 (the ratio of fluxes in step 4, the reduction of sulfite to S^{2+}—Fig. 1) is minimal (=0) and maximal (=1), respectively. The bottom right panel (d) is the calculated flux ratio of steps 1, 3 and 4 (Fig. 2.1—methods section) as a function of the cell specific sulfate reduction rate.

natural environment? This section addresses this question by applying our insights from pure culture experiments to $\delta^{18}O_{SO4}$ and $\delta^{34}S_{SO4}$ measured in sedimentary pore fluids. In this discussion, the depth below the seafloor of total consumption of sulfate is used to calculate the net sulfate reduction rate with the observation that sulfate is often consumed within three meters below the seafloor in environments with high sulfate reduction rates (on the order of 10^{-4}–10^{-5} mol cm^{-3} year^{-1}) such as estuaries and methane seeps (Aharon and Fu, 2000, 2003). On the other hand, sulfate is consumed at depths between three and ten meters in environments with moderate sulfate reduction rates (on the order of 10^{-6} mol cm^{-3} year^{-1}), including the continental shelf and river deltas (Aller et al., 2010). When sulfate is consumed deeper than ten meters below the seafloor, the environment is considered to have low sulfate reduction rates (lower than 10^{-7} mol cm^{-3} year^{-1}). The latter environments include organic-poor deep-sea sediments (Turchyn et al., 2006; Wortmann et al., 2007).

Fig. 7 plots $\delta^{18}O_{SO4}$ and $\delta^{34}S_{SO4}$ of pore fluids for these three types of sites (color coded), and overlays the curves for the relative evolution of $\delta^{18}O_{SO4}$ vs. $\delta^{34}S_{SO4}$ based on our experiments. Fig. 7 shows a number of notable features. First, the overall variation in the data from pore fluids follows our findings, where at lower rates of microbial sulfate reduction, the $\delta^{18}O_{SO4}$ increases rapidly relative to the $\delta^{34}S_{SO4}$. Second, most of the pore fluid data fall above our laboratory-derived estimate for kinetic oxygen isotope fractionation. Lastly, data points from at least eleven field sites with moderate to low sulfate reduction rates fall above the curve of our experiment with the slowest csSRR (glucose experiment) although this experiment is record the highest oxygen isotope fractionation (θ_o) in sulfate measured in pure culture to date.

In an open system such as marine sediments, transport (e.g. diffusion and advection through the pore fluids) should modify the measured $\delta^{18}O_{SO4}$ and $\delta^{34}S_{SO4}$ (Jørgensen, 1979; Wortmann et al., 2007; Chernyavsky and

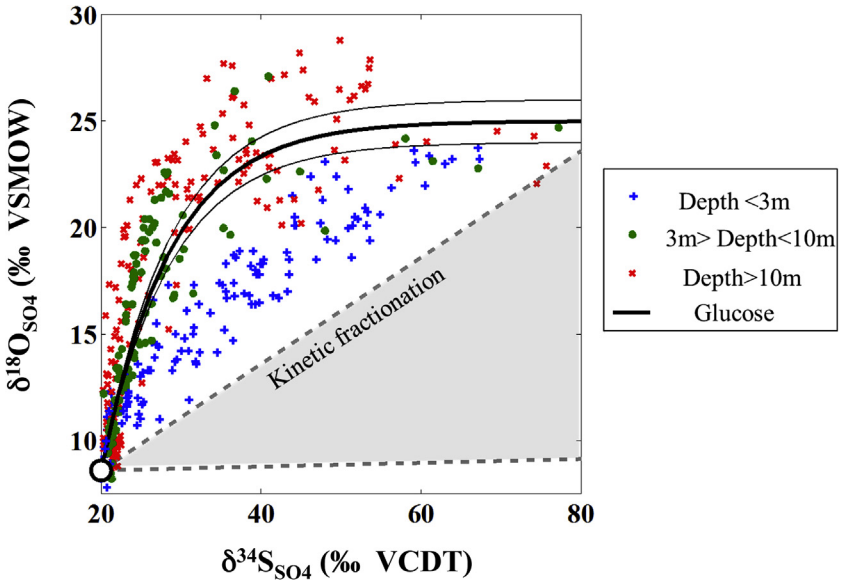

Fig. 7. $\delta^{18}O_{SO4}$ vs. $\delta^{34}S_{SO4}$ data from pore fluids. (Data were taken from Böttcher et al., 1998, 1999, 2006; Antler et al., 2013; Aharon and Fu, 2000, 2003; Blake et al., 2006; Turchyn et al., 2006, 2016; Wortmann et al., 2007; Wortmann, 2008; Aller et al., 2010; Wehrmann et al., 2011; Strauss et al., 2012). Broadly, the blue symbols (sulfate depletion above 3 m) are data from gas seeps sites and estuaries. The green symbols (sulfate depletion between 3 and 10 m) are data from continental shelf. The red symbols (sulfate depletion below 10 m) are data from deep-sea sediments. The area for 'kinetic fractionation' was calculated based on the fractionations of sulfur and oxygen in the lactate and malate experiment (Section 6.1). (For interpretation of the references to colour in this figure legend, the reader is referred to the web version of this article.)

Wortmann, 2007). Therefore, if we want to compare results from batch cultures (a closed system) to pore fluid data, it is important to consider the variations of $\delta^{18}O_{SO4}$ and $\delta^{34}S_{SO4}$ in open systems that are modified by transport. Given that the $\delta^{18}O_{SO4}$ vs. $\delta^{34}S_{SO4}$ relationship is always concave-down (except the special case when it is linear), by definition, any mixing between two points on the plot will results in a value lower than the original value. This means that the effect of transport can only result in a more moderate SALP. This effect was modelled by Antler et al. (2013). Therefore, transport (diffusion and advection) by itself cannot explain the discrepancy between our experiments and the pore water results and most likely will exacerbate this discrepancy.

Overall, pore fluids and pure culture experiments of microbial sulfate reducers exhibit similar trends. Some gaps between them can be explained by the much lower csSRR relative to the batch experiments (e.g. Holmkvist et al., 2011). However, some features, such as the high oxygen isotope equilibrium (which can be more than 5‰ higher than expected from our experiment—Fig. 7), with high apparent SALP in pore fluids from sites with slow sulfate reduction rates may not be explained only by MSR even if we consider any potential temperature effect on the oxygen isotope equilibrium between sulfur intermediates and water. Therefore, we suggest that different processes control this relationship in those cases. For instance, in gas seeps, where sulfate-driven anaerobic oxidation of methane is present, the plot of $\delta^{18}O_{SO4}$ and $\delta^{34}S_{SO4}$ shows a linear correlation with moderate slopes (Aharon and Fu, 2000, 2003; Rubin-Blum et al., 2014) due to little reoxidation of reduced sulfur species during net sulfate reduction (Antler et al., 2015). In contrast, in organic-poor sediments where the sulfate reduction rate is low and complex extracellular cycling between sulfur and iron, sulfur and manganese cycling or disproportionation is possible, the slopes of $\delta^{18}O_{SO4}$ vs. $\delta^{34}S_{SO4}$ are much steeper as $\delta^{18}O_{SO4}$ increases with minor changes in $\delta^{34}S_{SO4}$ (e.g. Böttcher and Thamdrup, 2001; Böttcher et al., 2001, 2005; Blake et al., 2006; Aller et al., 2010; Mills et al., 2016). From this perspective, oxygen isotopes in sulfate are a more reliable indicator of extracellular reoxidation than sulfur isotopes. An alternative speculation is that with extreme low availability of organic carbon, DsrC is also much less available, which might result in the formation of other intermediates including trithionate ($S_4O_6^{2-}$) and thiosulfate ($S_2O_3^{-2}$) (Bradley et al., 2011; Santos et al., 2015) which will ultimately will alter the oxygen and sulfur isotope fractionation.

The next challenge will be to resolve the gap between the pure cultures experiments and *in situ* pore fluid $\delta^{34}S_{SO4}$ and $\delta^{18}O_{SO4}$. This might be enabled by the increasing the availability of coupled measurements of $\delta^{34}S_{SO4}$, $\delta^{33}S_{SO4}$ and $\delta^{18}O_{SO4}$ values together with csSRR. Studies of microbial cultures at even lower csSRR may also yield even higher $\delta^{34}S_{SO4}$, $\delta^{33}S_{SO4}$ and $\delta^{18}O_{SO4}$ signals and expand the known range of oxygen and sulfur isotope fractionations accessible to MSR.

6. SUMMARY

This study presents measurements of $^{33}S/^{32}S$, $^{34}S/^{32}S$ and $^{18}O/^{16}O$ in pure cultures of *Desulfovibrio* sp. (strain

DMSS-1). The cell-specific sulfate reduction rates vary over three orders of magnitude in DMSS-1 cultures growing on these different electron donors. The data show that isotopic fractionations of sulfur and oxygen isotopes in dissolved sulfate record different processes under controlled conditions and depend on sulfate reduction rates. As previously shown, the $^{34}S/^{32}S$ isotope fractionation varies between 7‰ and 61‰ and correlates with the cell specific sulfate reduction rates. The combination of sulfur and oxygen isotope data also demonstrates for that the values of oxygen isotope fractionation at apparent equilibrium are a function of the cell specific sulfate reduction rates. These results are used to calculate the ratios of fluxes at each individual step during microbial sulfate reduction.

Compared to the previously reported environmental observations, the culture results cannot explain some combinations of sulfur and oxygen isotope fractionations in nature. We propose that the gap between lab experiments and the natural environment may arise from the much lower availability of organic matter in nature than culture. In addition, processes such as the oxidation of intermediate sulfur redox species to sulfate, sulfur disproportionation and sulfate-driven anaerobic methane oxidation likely impact the isotopic correlation in the environment, but not in pure cultures of sulfate reducing microbes. Experiments with natural populations and sulfate reducers limited by very low concentrations of organic matter can explore the combined effects of processes that impart isotopic signatures on sulfur and oxygen in dissolved sulfate.

ACKNOWLEDGEMENTS

This study could not have been done without the technical support of Efrat Eliani-Russak from Ben Gurion University of the Negev, James Rolfe from the Godwin Laboratory at the University of Cambridge and Bill Olszewski from Massachusetts Institute of Technology Stable Isotope Geobiology Laboratory. We are in debt with David T. Wang and Min Sub Sim for their help and discussion. The authors also thanks the two anonymous reviewers for constructive reviews that greatly improved this manuscript. This study was funded by NAI Complex Life (#NNA08CN84A) to Tanja Bosak and NSF (EAR-1159318) to Shuhei Ono and Tanja Bosak and the European Research Council Starting Grant (CARBONSINK, 307582) to Alexandra V. Turchyn.

APPENDIX 1. NOTATIONS

Sulfur has four natural occurring isotopes (with relative abundances shown in brackets); ^{32}S (95.039%), ^{33}S (0.748%), ^{34}S (4.197%) and ^{36}S (0.014%). Oxygen has three natural occurring isotopes; ^{16}O (99.759%) ^{17}O (0.037%) and ^{18}O (0.204%). Stable isotope ratios (e.g. for ^{34}S over ^{32}S), are commonly reported using δ notation, give as:

$$\delta^{34}S = \left(\frac{R_{sample} - R_{VCDT}}{R_{VCDT}}\right) \cdot 1000 \quad (A.1)$$

where R_{sample} and R_{CDT} are the ratios between the heavier and the lighter isotopes in a sample and an internationally recognized standard (for sulfur the standard is Vienna Canyon Diablo Troilite—VCDT and for oxygen the standard is Vienna Standard Mean Ocean Water—VSMOW). Delta notation is used for reporting isotope ratios because the variation in the ratio is largely in the 'parts per thousand' or permil (‰), range. The fractionation factor (α) between the product (H_2S) and substrate (SO_4^{2-}) is therefore defined as:

$$\alpha^{34}S = \frac{R_{H2S}}{R_{SO4}} \quad (A.2)$$

and the isotope fractionation (ε), given in permil, defined as:

$$\varepsilon^{34}S = 1000 \cdot \ln(\alpha^{34}S) \quad (A.3)$$

APPENDIX 2. DATA PROCESSING

2.1. Calculation of cell-specific sulfate reduction rate

Many previous studies have addressed the relationship between the sulfate reduction rate (or more specifically the cell specific sulfate reduction rate) and the magnitude of sulfur isotope fractionation. The average cell-specific sulfate reduction rate (often abbreviated as csSRR) is calculated from the ratio between the specific growth rate and the growth yield (after Sim et al., 2011a,b, who explain why this is more appropriate than the assumption of linear growth). The specific growth rate (K) was calculated based on the slope on the plot between ln(cells) vs. time:

$$K = \frac{d\ln(c)}{dt} \quad (A.4)$$

where c is the cell density (cells/ml) and t is time. The growth yield (Y) was calculated based on the slope on the plot between cells vs. sulfide:

$$Y = \frac{dc}{dSO_4^{2-}} \quad (A.5)$$

csSRR is therefore equal to:

$$csSRR = \frac{K}{Y} \quad (A.6)$$

2.2. Sulfur isotope fractionation

The isotope fractionation (ε) in the batch culture experiment was calculated using the Rayleigh distillation equation:

$$\varepsilon^{3x}S = \left(-\frac{1}{\ln(f_r)}\ln\left(\frac{\frac{\delta^{3x}S_0}{1000}+1}{\frac{\delta^{3x}S}{1000}+1}\right)\right) \cdot 1000 \quad (A.7)$$

where f_r is the fraction of the remaining sulfate, and $\delta^{3x}S_0$ and $\delta^{3x}S$ are sulfur isotope compositions (^{33}S or ^{34}S) of the sulfate at time 0 and the sulfate remaining at the time of sampling, respectively.

2.3. Calculating $\delta^{18}O_{SO4(A.E)}$ and θ_O

Given that $\delta^{18}O_{SO4}$ does not always reach apparent equilibrium within the frame of given experiment or in the natural environment, the apparent equilibrium value

($\delta^{18}O_{SO4(A.E)}$) can be obtained from the correlation of SALP and $\delta^{18}O_{SO4(A.E)}$ (Eq. (7)); this correlation implies that one can calculate $\delta^{18}O_{SO4(A.E)}$ from the cross plot of SALP vs. $\delta^{18}O_{H2O}$. At the intercept of a SALP vs. $\delta^{18}O_{H2O}$ line ($\delta^{18}O_{H2O} = 0$), the $\delta^{18}O_{SO4(A.E)}$ is equal to:

$$\delta^{18}O_{SO4(A.E)} = SALP_{(\delta^{18}O_{H2O}=0)} \frac{\varepsilon^{34}S_{total}}{\theta_O} + \delta^{18}O_{SO4(t=0)} \quad (A.8)$$

where $SALP(\delta^{18}O_{H2O} = 0)$ is the slope of the apparent linear phase predicted at $\delta^{18}O_{H2O} = 0$ (and the intercept on the SALP vs. $\delta^{18}O_{H2O}$ plot) and $\delta^{18}O_{SO4(t=0)}$ is the initial $\delta^{18}O_{SO4}$ value (at time zero).

Similarly, a useful way to study the mutual evolution of $\delta^{18}O_{SO4}$ and $\delta^{34}S_{SO4}$ with respect to the progress of reaction (e.g. the decrease in sulfate concentration with time during MSR) is to plot θ_O vs. $\varepsilon^{34}S_{total}$ (Fig. 2b). Previous studies have used this cross-plot to investigate the mechanism of MSR (Brunner et al., 2005, 2012; Knöller et al., 2006; Turchyn et al., 2010; Antler et al., 2013) and sulfate-driven anaerobic methane oxidation (Deusner et al., 2014). Because both $\varepsilon^{34}S_{total}$ and θ_O are functions of the forward and backward fluxes during MSR (Eqs. (6) and (9), respectively), this plot can be used to relate sulfur and oxygen isotope measurements to the intracellular MSR fluxes. This is because for every set of given forward and backward fluxes there are specific values of θ_O and $\varepsilon^{34}S_{total}$. However, because there are more branching points in the framework of MSR than the solution for θ_O and $\varepsilon^{34}S_{total}$, the ratio of between the forward and backward fluxes of every branching point cannot be solved uniquely. Fig. 2b also demonstrates the relationship between θ_O vs. $\varepsilon^{34}S_{total}$ and the ratio of intracellular fluxes.

Calculations of θ_O must assume a certain value of $\delta^{18}O_{SO4(A.E)}$ (e.g. Brunner et al., 2006; Knöller et al., 2006—see also Eq. (5)). However, if the value of $\delta^{18}O_{SO4}$ does not reach equilibrium, there might be a big uncertainty in estimating the value of $\delta^{18}O_{SO4(A.E)}$. Alternatively, θ_O can be estimated without assuming the $\delta^{18}O_{SO4(A.E)}$ value; here, we resolve this by noting that $\delta^{18}O_{SO4(A.E)}$ is proportional to the $\delta^{18}O_{H2O}$ (Eq. (8)), and their differentials are equal: $d(\delta^{18}O_{SO4(A.E)}) = d(\delta^{18}O_{H2O})$, therefore they are directly proportional. In addition, the slope of the apparent linear phase (SALP) is proportional to $\delta^{18}O_{SO4(A.E)}$ (Eq. (7)). Hence, if we combine these two constrains, the SALP is also proportional to $\delta^{18}O_{H2O}$:

$$SALP \propto \delta^{18}O_{H2O} \quad (A.9)$$

According to Eq. (7), the proportionality coefficient should be equal to $\theta_O/\varepsilon^{34}S_{total}$ and is equal to the slope of the SALP vs. $\delta^{18}O_{H2O}$. Then, $\varepsilon^{34}S_{total}$ is easily calculated from experimental measurements, and θ_O can be derived.

APPENDIX 3. $\delta^{18}O$ MEASUREMENT VALIDATION

Growth experiments used enriched ^{18}O water (with $\delta^{18}O_{H2O}$ up to ~78‰), which introduces several analytical issues. First, it is not clear how linear the mass spectrometers are for high values of $\delta^{18}O_{H2O}$ and $\delta^{18}O_{SO4}$. A non-linear response will result in error in the analysis since our isotope measurements are often exceeding the calibration envelope. We resolved this by diluting the high samples with a standard with low oxygen isotopic composition (−7.3‰ and −11.35‰ for $\delta^{18}O_{H2O}$ and $\delta^{18}O_{SO4}$, respectively). An example is shown in Fig. A1. Both $\delta^{18}O_{H2O}$ and $\delta^{18}O_{SO4}$, are shown with the mixing line between the high $\delta^{18}O$ sample and the low $\delta^{18}O$ standard. This exercise demonstrates that there is no significant effect on the $\delta^{18}O_{H2O}$ and $\delta^{18}O_{SO4}$ measurements as far from the calibration envelope as our experiments were done.

An example is shown in Fig. A.2. Both $\delta^{18}O_{H2O}$ and $\delta^{18}O_{SO4}$, are shown with the mixing line between the high $\delta^{18}O$ sample and the low $\delta^{18}O$ standard. This exercise demonstrates that there is no significant effect on the $\delta^{18}O_{H2O}$ and $\delta^{18}O_{SO4}$ measurements as far from the calibration envelope as our experiments were done.

The second potential problem with using high $\delta^{18}O_{H2O}$ is the incorporation of water molecules into the barite crystal lattice. In order to examine the effect of the ^{18}O-enriched

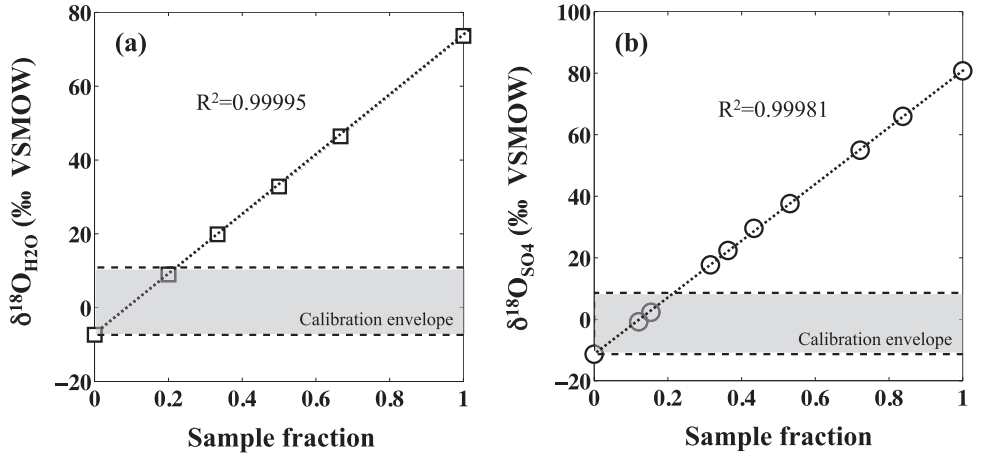

Fig. A1. Measured $\delta^{18}O_{H2O}$ values (a) and $\delta^{18}O_{SO4}$ values (b) plotted versus sample dilution with a low value standard. The sample fraction is the fraction of the sample in the final mixture between the sample and the low standard.

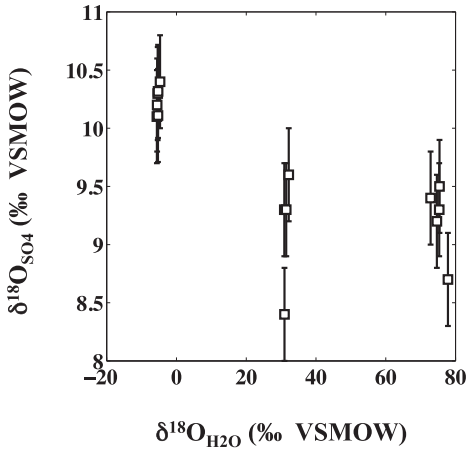

Fig. A2. The initial $\delta^{18}O_{SO4}$ of each experiment compared to the ambient $\delta^{18}O_{H2O}$.

water on the measurement, we compare the initial $\delta^{18}O_{SO4}$ from all our experiment versus the $\delta^{18}O_{H2O}$ of the solution (Fig. A.2). From this we show that the highest $\delta^{18}O_{SO4}$ we measure are, ironically, in the lowest $\delta^{18}O_{H2O}$, in addition there is no significant difference between $\delta^{18}O_{SO4}$ that was measured with water that had a $\delta^{18}O_{H2O}$ of ~75‰ or ~35‰ (Fig. A.2). This suggests that, for this experimental setup, there is virtually no effect of the oxygen isotopic composition of water on the oxygen isotopic composition of the sulfate during laboratory handling. We suggest that the high $\delta^{18}O_{SO4}$ value in the experiment with low $\delta^{18}O_{H2O}$ is most likely due to different batches of Na_2SO_4 salt that were used, which is also supported by different initial $\delta^{34}S_{SO4}$ (Supplementary) which is ~1‰ in the experiments with higher the $\delta^{18}O_{SO4}$.

APPENDIX B. SUPPLEMENTARY DATA

Supplementary data associated with this article can be found, in the online version, at http://dx.doi.org/10.1016/j.gca.2017.01.015.

REFERENCES

Avrahamov N., Antler G., Yechieli Y., Gavrieli I., Joye S. B., Saxton M., Turchyn A. V. and Sivan O. (2014) Anaerobic oxidation of methane by sulfate in hypersaline groundwater of the Dead Sea aquifer. *Geobiology* **12**, 511–528.

Aharon P. and Fu B. (2000) Microbial sulfate reduction rates and sulfur and oxygen isotope fractionations at oil and gas seeps in deepwater Gulf of Mexico. *Geochim. Cosmochim. Acta* **64**, 233–246.

Aharon P. and Fu B. (2003) Sulfur and oxygen isotopes of coeval sulfate–sulfide in pore fluids of cold seep sediments with sharp redox gradients. *Chem. Geol.* **195**, 201–218.

Akagi J. M. (1995) Respiratory sulfate reduction. In *Sulfate-Reducing Bacteria*, pp. 89–111. Sulfate-Reducing Bacteria. Springer, US.

Aller R. C., Madrid V., Chistoserdov A., Aller J. Y. and Heilbrun C. (2010) Unsteady diagenetic processes and sulfur biogeochemistry in tropical deltaic muds: implications for oceanic isotope cycles and the sedimentary record. *Geochim. Cosmochim. Acta* **74**, 4671–4692.

Antler G., Turchyn A. V., Rennie V., Herut B. and Sivan O. (2013) Coupled sulfur and oxygen isotope insight into bacterial sulfate reduction in the natural environment. *Geochim. Cosmochim. Acta* **118**, 98–117.

Antler G., Turchyn A. V., Herut B., Davies A., Rennie V. and Sivan O. (2014) Sulfur and oxygen isotope tracing of sulfate driven anaerobic methane oxidation in estuarine sediments. *Estuar. Coast. Shelf Sci.* **142**, 4–11.

Antler G., Turchyn A. V., Herut B. and Sivan O. A. (2015) Unique isotopic fingerprint of sulfate-driven anaerobic oxidation of methane. *Geology* **43**, 619–622.

Balci N., Shanks W., Bernhard M. and Mandernack K. (2007) Oxygen and sulfur isotope systematics of sulfate produced by bacterial and abiotic oxidation of pyrite. *Geochim. Chosmochim. Acta* **71**, 3796–3811.

Betts R. H. and Voss R. H. (1970) The kinetics of oxygen exchange between the sulfite ion and water. *Can. J. Chem.* **48**, 2035–2041.

Blake R. E., Surkov A. V., Böttcher M. E., Ferdelman T. G. and Jørgensen B. B. (2006) Oxygen isotope composition of dissolved sulfate in deep-sea sediments: Eastern Equatorial Pacific Ocean. In *Proc Ocean Drill Prog Sci Results*, vol. 201 (eds. B. B. Jørgensen, S. L. D'Hondt and D. J. Miller). ODP, pp. 1–24.

Böttcher M. E. and Thamdrup B. (2001) Anaerobic sulfide oxidation and stable isotope fractionation associated with bacterial sulfur disproportionation in the presence of MnO_2. *Geochim. Cosmochim. Acta* **65**, 1573–1581.

Böttcher M. E., Brumsack H. J. and de Lange G. J. (1998) Sulfate reduction and related stable isotope (^{34}S, ^{18}O) variations in interstitial waters from the eastern Mediterranean. In *Proc. ODP, Sci. Results*, 160 (eds. A. H. F. Robertson, K.-C. Emeis, C. Richter and A. Camerlenghi). Ocean Drilling Program, College Station, TX, pp. 365–373.

Böttcher M. E., Bernasconi S. M. and Brumsack H. J. (1999) Carbon, sulfur, and oxygen isotope geochemistry of interstitial waters from the western Mediterranean. In *Proceedings of the Ocean Drilling Program, Scientific Results*, vol. 161 (eds. R. Zahn, M. C. Comas and A. Klaus). Proc Ocean Drill Prog Sci Results. Ocean Drilling Program, College Station, TX, pp. 413–421.

Böttcher M. E., Thamdrup B. and Vennemann T. W. (2001) Oxygen and sulfur isotope fractionation during anaerobic bacterial disproportionation of elemental sulfur. *Geochim. Cosmochim. Acta* **65**, 1601–1609.

Böttcher M. E., Thamdrup B., Gehre M. and Theune A. (2005) 34S/32S and 18O/16O fractionation during sulfur disproportionation by *Desulfobulbus propionicus*. *Geomicrobiol. J.* **22**, 219.

Böttcher M. E., Ferdelman T. G., Jørgensen B. B., Blake R. E., Surkov A. V. and Claypool G. E. (2006) Sulfur isotope fractionation by the deep biosphere within sediments of the Eastern Equatorial Pacific and Peru Margin. In *Proc Ocean Drill Prog Sci Results*, vol. 201 (eds. B. B. Jørgensen, S. L. D'Hondt and D. J. Miller). ODP, pp. 1–21.

Bowles M. W., Mogollón J. M., Kasten S., Zabel M. and Hinrichs K. U. (2014) Global rates of marine sulfate reduction and implications for sub-sea-floor metabolic activities. *Science* **344**, 889–891.

Bradley A. S., Leavitt W. D. and Johnston D. T. (2011) Revisiting the dissimilatory sulfate reduction pathway. *Geobiology* **9**, 446–457.

Bradley A. S., Leavitt W. D., Schmidt M., Knoll A. H., Girguis P. R. and Johnston D. T. (2016) Patterns of sulfur isotope fractionation during microbial sulfate reduction. *Geobiology* **14**, 91–101.

Brüchert V. (2004) Physiological and ecological aspects of sulfur isotope fractionation during bacterial sulfate reduction. In *Sulfur Biogeochemistry – Past and Present*, vol. 379 (eds. J. P. Amend, K. J. Edwards and T. W. Lyons). Geological Society of America Special Paper. Geol. Soc. Am, Boulder CO, USA, pp. 1–16.

Brunner B. and Bernasconi S. M. (2005) A revised isotope fractionation model for dissimilatory sulfate reducing in sulfate reducing bacteria. *Geochim. Cosmochim. Acta* **69**, 4759–4771.

Brunner B., Bernasconi S. M., Kleikemper J. and Schroth M. J. (2005) A model for oxygen and sulfur isotope fractionation in sulfate during bacterial sulfate reduction processes. *Geochim. Cosmochim. Acta* **69**, 4773–4785.

Brunner B., Yu J.-Y., Mielke R., MacAskill J., Madzunkov S., McGenity T. and Coleman M. (2008) Different isotope and chemical patterns of pyrite oxidation related to lag and exponential growth phases of *Acidithiobacillus ferrooxidans* reveal a microbial growth strategy. *Earth Planet. Sci. Lett.* **270**, 63–72.

Brunner B., Einsiedl F., Arnold G. L., Müller I., Templer S. and Bernasconi S. M. (2012) The reversibility of dissimilatory sulphate reduction and the cell-internal multi-step reduction of sulphite to sulphide: insights from the oxygen isotope composition of sulphate. *Isot. Environ. Health Stud.* **48**, 33–54.

Canfield D. E. (2001a) Biogeochemistry of sulfur isotopes. In *Reviews in Mineralogy and Geochemistry*, vol. 43 (eds. J. W. Valley and D. R. Cole), pp. 607–636. Reviews in Mineralogy and Geochemistry. Mineral. Soc. Am, Blacksburg, VA.

Canfield D. E. (2001b) Isotope fractionation by natural populations of sulfate-reducing bacteria. *Geochim. Cosmochim. Acta* **65**, 1117–1124.

Canfield D. E. (2004) The evolution of the earth surface sulfur reservoir. *Am. J. Sci.* **304**, 839–861.

Canfield D. E., Olesen C. A. and Cox R. P. (2006) Temperature and its control of isotope fractionation by a sulfate-reducing bacterium. *Geochim. Cosmochim. Acta* **70**, 548–561.

Canfield D. E., Farquhar J. and Zerkle A. L. (2010) High isotope fractionations during sulfate reduction in a low-sulfate euxinic ocean analog. *Geology* **38**, 415–418.

Chambers L. A., Trudinger P. A., Smith J. W. and Burns M. S. (1975) Fractionation of sulfur isotopes by continuous cultures of *Desulfovibrio desulfuricans*. *Can. J. Microbiol.* **21**, 1602–1607.

Chernyavsky B. M. and Wortmann U. G. (2007) REMAP: a reaction transport model for isotope ratio calculations in porous media. *Geochem. Geophys. Geosyst.* **8**.

Chiba H. and Sakai H. (1985) Oxygen isotope exchange-rate between dissolved sulfate and water at hydrothermal temperatures. *Geochim. Cosmochim. Acta* **49**, 993–1000.

Cline J. D. (1969) Spectrophotometric determination of hydrogen sulfide in natural water. *Limnol. Oceanogr.* **14**, 454–458.

Cypionka H., Smock A. and Böttcher M. E. (1998) A combined pathway of sulfur compound disproportionation in *Desulfovibrio desulfuricans*. *FEMS Microbiol. Lett.* **166**, 181–186.

Deusner C., Holler T., Arnold G. L., Bernasconi S. M., Formolo M. J. and Brunner B. (2014) Sulfur and oxygen isotope fractionation during sulfate reduction coupled to anaerobic oxidation of methane is dependent on methane concentration. *Earth Planet. Sci. Lett.* **399**, 61–73.

Eckert T., Brunner B., Edwards E. A. and Wortmann U. G. (2011) Microbially mediated re-oxidation of sulfide during dissimilatory sulfate reduction by *Desulfobacter latus*. *Geochim. Cosmochim. Acta* **75**, 3469–3485.

Farquhar J., Johnston D. T., Wing B. A., Habicht K. S., Canfield D. E., Airieau S. and Thiemens M. H. (2003) Multiple sulphur isotopic interpretations of biosynthetic pathways: implications for biological signatures in the sulphur isotope record. *Geobiology* **1**, 27–36.

Farquhar J., Johnston D. T. and Wing B. A. (2007) Implications of conservation of mass effects on mass-dependent isotope fractionations: influence of network structure on sulfur isotope phase space of dissimilatory sulfate reduction. *Geochim. Cosmochim. Acta* **71**, 5862–5875.

Farquhar J., Canfield D. E., Masterson A., Bao H. and Johnston D. (2008) Sulfur and oxygen isotope study of sulfate reduction in experiments with natural populations from Fællestrand, Denmark. *Geochim. Cosmochim. Acta* **72**, 2805–2821.

Fitz R. M. and Cypionka H. (1990) Formation of thiosulfate and trithionate during sulfite reduction by washed cells of *Desulfovibrio desulfuricans*. *Arch. Microbiol.* **154**, 400–406.

Fritz P., Basharmal G. M., Drimmie R. J., Ibsen J. and Qureshi R. M. (1989) Oxygen isotope exchange between sulfate and water during bacterial reduction of sulfate. *Chem. Geol.* **79**, 99–105.

Gilhooly W. P., Reinhard C. T. and Lyons T. W. (2016) A comprehensive sulfur and oxygen isotope study of sulfur cycling in a shallow, hyper-euxinic meromictic lake. *Geochim. Cosmochim. Acta* **189**, 1–23.

Habicht K. S., Gade M., Thamdrup B., Berg P. and Canfield D. E. (2002) Calibration of sulphate levels in the Archean Ocean. *Science* **298**, 2372–2374.

Harrison A. G. and Thode H. G. (1958) Mechanism of the bacterial reduction of sulphate from isotope fractionation studies. *Trans. Faraday Soc.* **53**, 84–92.

Heidel C. and Tichomirowa M. (2011) The isotopic composition of sulfate from anaerobic and low oxygen pyrite oxidation experiments with ferric iron – new insights into oxidation mechanisms. *Chem. Geol.* **281**, 305–316.

Hilz H. and Lipmann F. (1955) The enzymatic activation of sulfate. *Proc. Natl. Acad. Sci. U.S.A.* **41**, 880.

Hoek J., Reysenbach A. L., Habicht K. S. and Canfield D. E. (2006) Effect of hydrogen limitation and temperature on the fractionation of sulfur isotopes by a deep-sea hydrothermal vent sulfate-reducing bacterium. *Geochim. Cosmochim. Acta* **70**, 5831–5841.

Holler T., Wegener G., Niemann H., Deusner C., Ferdelman T. G., Boetius A., Brunner B. and Widdel F. (2011) Carbon and sulfur back flux during anaerobic microbial oxidation of methane and coupled sulfate reduction. *Proc. Natl. Acad. Sci. U.S.A.* **108**, 1484–1490.

Holmkvist L., Ferdelman T. G. and Jørgensen B. B. (2011) A cryptic sulfur cycle driven by iron in the methane zone of marine sediment (Aarhus Bay, Denmark). *Geochim. Cosmochim. Acta* **75**, 3581–3599.

Horner D. A. and Connick R. E. (2003) Kinetics of oxygen exchange between the two isomers of bisulfite ion, disulfite ion ($S_2O_5^{2-}$), and water as studied by oxygen-17 nuclear magnetic resonance spectroscopy. *Inorg. Chem.* **42**, 1884–1894.

Johnston D. T., Wing B. A., Farquhar J., Kaufman A. J., Strauss H., Lyons T. W. and Canfield D. E. (2005) Active microbial sulfur disproportionation in the Mesoproterozoic. *Science* **310**, 1477–1479.

Johnston D. T., Farquhar J. and Canfield D. E. (2007) Sulfur isotope insights into microbial sulfate reduction: when microbes meet model. *Geochim. Cosmochim. Acta* **71**, 3929–3947.

Johnston D. T., Gill B., Masterson A., Beirne E., Casciotti K., Knapp A. and Berelson W. (2014) Placing an upper limit on cryptic marine sulphur cycling. *Nature* **513**, 530–533.

Jørgensen B. B. (1979) A theoretical model of the stable sulfur isotope distribution in marine sediments. *Geochim. Cosmochim. Acta* **43**, 363–374.

Kamyshny A., Zerkle A. L., Mansaray Z. F., Ciglenečki I., Bura-Nakić E., Farquhar J. and Ferdelman T. G. (2011) Biogeochemical sulfur cycling in the water column of a shallow

stratified sea-water lake: speciation and quadruple sulfur isotope composition. *Mar. Chem.* **127**, 144–154.
Kaplan I. R. and Rittenberg S. C. (1963) Microbiological fractionation of sulphur isotopes. *J. Gen. Microbiol.* **34**, 195–212.
Kasten S. and Jørgensen B. B. (2000) Sulfate reduction in marine sediments. In *Marine Geochemistry* (eds. H. D. Schulz and M. Zabel). Springer, Berlin.
Knöller K., Vogt C., Richnow H. H. and Weise S. M. (2006) Sulfur and oxygen isotope fractionation during benzene, toluene, ethyl benzene, and xylene degradation by sulfate-reducing bacteria. *Environ. Sci. Technol.* **40**, 3879–3885.
Knossow N., Blonder B., Eckert W., Turchyn A. V., Antler G. and Kamyshny A. (2015) Annual sulfur cycle in a warm monomictic lake with sub-millimolar sulfate concentrations. *Geochem. Trans.* **16**, 7.
Kobayashi K., Tachibana S. and Ishimoto M. (1969) Intermediary formation of trithionate in sulfite reduction by a sulfate-reducing bacterium. *J. Biochem. (Tokyo)* **65**, 155.
Kohl I. E. and Bao H. (2011) Triple-oxygen-isotope determination of molecular oxygen incorporation in sulfate produced during abiotic pyrite oxidation (pH = 2–11). *Geochim. Cosmochim. Acta* **75**, 1785–1798.
Kohl I. E., Asatryan R. and Bao H. (2012) No oxygen isotope exchange between water and APS–sulfate at surface temperature: evidence from quantum chemical modeling and triple-oxygen isotope experiments. *Geochim. Cosmochim. Acta* **95**, 106–118.
Leavitt W. D., Halevy I., Bradley A. S. and Johnston D. T. (2013) Influence of sulfate reduction rates on the Phanerozoic sulfur isotope record. *Proc. Natl. Acad. Sci. U.S.A.* **110**, 11244–11249.
Leavitt W. D., Cummins R., Schmidt M. L., Sim M. S., Ono S., Bradley A. S. and Johnston D. T. (2014) Multiple sulfur isotope signatures of sulfite and thiosulfate reduction by the model dissimilatory sulfate-reducer Desulfovibrio alaskensis str. G20. *Front. Microbiol.* **5**.
Leavitt W. D., Bradley A. S., Santos A. A., Pereira I. A. and Johnston D. T. (2015) Sulfur isotope effects of dissimilatory sulfite reductase. *Front. Microbiol* **6**.
Lloyd R. M. (1968) Oxygen isotope behavior in sulfate–water system. *J. Geophys. Res.* **73**, 6099–6110.
Mandernack K., Krouse H. R. and Skei J. M. (2003) A stable sulfur and oxygen isotopic investigation of sulfur cycling in an anoxic marine basin, Framvaren Fjord, Norway. *Chem. Geol.* **195**, 181–200.
Mangalo M., Meckenstock R. U., Stichler W. and Einsiedl F. (2007) Stable isotope fractionation during bacterial sulfate reduction is controlled by reoxidation of intermediates. *Geochim. Cosmochim. Acta* **71**, 4161–4171.
Mangalo M., Einsiedl F., Meckenstock R. U. and Stichler W. (2008) Influence of the enzyme dissimilatory sulfite reductase on stable isotope fractionation during sulfate reduction. *Geochim. Cosmochim. Acta* **71**, 4161–4171.
Michaels G. B., Davidson J. T. and Peck H. D. (1970) A flavin-sulfite adduct as an intermediate in the reaction catalyzed by adenylyl sulfate reductase from Desulfovibriovulgaris. *Biochem. Biophys. Res. Commun.* **39**, 321–328.
Mills J. V., Antler G. and Turchyn A. V. (2016) Geochemical evidence for cryptic sulfur cycling in salt marsh sediments. *Earth Planet. Sci. Lett.* **453**, 23–32.
Mikucki J. A., Pearson A., Johnston D. T., Turchyn A. V., Farquhar J., Schrag D. P. and Lee P. A. (2009) A contemporary microbially maintained subglacial ferrous ocean. *Science* **324** (5925), 397–400.
Mizutani Y. and Rafter T. A. (1973) Isotopic behavior of sulphate oxygen in the bacterial reduction of sulphate. *Geochem. J.* **6**, 183–191.
Mizutani Y. and Rafter T. A. (1969) Oxygen isotopic composition of sulphates – Part 4; bacterial fractionation of oxygen isotopes in the reduction of sulphates and in the oxidation of sulphur. *N. Z. J. Sci.* **12**, 60–68.
Müller I. A., Brunner B., Breuer C., Coleman M. and Bach W. (2013) The oxygen isotope equilibrium fractionation between sulfite species and water. *Geochim. Cosmochim. Acta* **120**, 562–581.
Oliveira T. F., Vonrhein C., Matias P. M., Venceslau S. S., Pereira I. A. and Archer M. (2008) The crystal structure of *Desulfovibrio vulgaris* dissimilatory sulfite reductase bound to DsrC provides novel insights into the mechanism of sulfate respiration. *J. Biol. Chem.* **283**, 34141–34149.
Ono S., Wing B., Johnston D., Farquhar J. and Rumble D. (2006) Mass-dependent fractionation of quadruple stable sulfur isotope system as a new tracer of sulfur biogeochemical cycles. *Geochim. Cosmochim. Acta* **70**, 2238–2252.
Ono S., Sim M. S. and Bosak T. (2014) Predictive isotope model connects microbes in culture and nature. *Proc. Natl. Acad. Sci. U.S.A.* **111**, 18102–18103.
Pellerin A., Anderson-Trocmé L., Whyte L. G., Zane G. M., Wall J. D. and Wing B. A. (2015a) Sulfur isotope fractionation during the evolutionary adaptation of a sulfate-reducing bacterium. *Appl. Environ. Microbiol.* **81**, 2676–2689.
Pellerin A., Bui T. H., Rough M., Mucci A., Canfield D. E. and Wing B. A. (2015b) Mass-dependent sulfur isotope fractionation during reoxidative sulfur cycling: a case study from Mangrove Lake, Bermuda. *Geochim. Cosmochim. Acta* **149**, 152–164.
Pierik A. J., Hagen W. R., Redeker J. S., Wolbert R. B., Boersma M., Verhagen M. F., Grande H. J., Veeger C., Mutsaers P. H., Sands R. H. and Dunham W. R. (1992) Redox properties of the iron-sulfur clusters in activated Fe-hydrogenase from *Desulfovibrio vulgaris* (Hildenborough). *Eur. J. Biochem.* **209**, 63–72.
Piłsyk S. and Paszewski A. (2009) Sulfate permeases—phylogenetic diversity of sulfate transport. *Acta Biochim. Pol.* **56**, 375–384.
Poser A., Vogt C., Knöller K., Sorokin D., Finster K. and Richnow H. (2016) Sulfur and oxygen isotope fractionation during bacterial sulfur disproportionation under anaerobic haloalkaline conditions. *Geomicrobiol J.* (accepted).
Rees C. E. (1973) A steady-state model for sulphur isotope fractionation in bacterial reduction processes. *Geochim. Cosmochim. Acta* **37**, 1141–1162.
Rennie V. C. and Turchyn A. V. (2014) The preservation of and in carbonate-associated sulfate during marine diagenesis: a 25 Myr test case using marine sediments. *Earth Planet. Sci. Lett.* **395**, 13–23.
Riedinger N., Brunner B., Formolo M. J., Solomon E., Kasten S., Strasser M. and Ferdelman T. G. (2010) Oxidative sulfur cycling in the deep biosphere of the Nankai Trough, Japan. *Geology* **38**, 851–854.
Rubin-Blum M. et al. (2014) Hydrocarbon-related microbial processes in the deep sediments of the Eastern Mediterranean Levantine Basin. *FEMS Microbiol. Ecol.* **87**, 780–796.
Santos A. A., Venceslau S. S., Grein F., Leavitt W. D., Dahl C., Johnston D. T. and Pereira I. A. (2015) A protein trisulfide couples dissimilatory sulfate reduction to energy conservation. *Science* **350**, 1541–1545.
Sim M. S., Bosak T. and Ono S. (2011a) Large sulfur isotope fractionation does not require disproportionation. *Science* **333**, 74–77.
Sim M. S., Ono S., Donovan K., Templer S. P. and Bosak T. (2011b) Effect of electron donors on the fractionation of sulfur isotopes by a marine *Desulfovibrio* sp. *Geochim. Cosmochim. Acta* **75**, 4244–4259.
Sim M. S., Liang B., Petroff A. P., Evans A., Klepac-Ceraj V., Flannery D. T., Walter M. R. and Bosak T. (2012) Oxygen-dependent morphogenesis of modern clumped photosynthetic

mats and implications for the Archean stromatolite record. *Geosciences* **2**, 235–259.
Sim M. S., Wang D. T., Zane G. M., Wall J. D., Bosak T. and Ono S. (2013) Fractionation of sulfur isotopes by *Desulfovibrio vulgaris* mutants lacking hydrogenases or type I tetraheme cytochrome c3. *Front. Microbiol.* **4**.
Sivan O., Antler G., Turchyn A. V., Marlow J. and Orphan V. J. (2014) Iron oxides stimulate sulfate driven anaerobic methane oxidation in seeps. *Proc. Natl. Acad. Sci. U.S.A.* **111**, E4139–E4147.
Strauss H. et al. (2012) Sulphur diagenesis in the sediments of the Kiel Bight, SW Baltic Sea, as reflected by multiple stable sulphur isotopes. *Isot. Environ. Health Stud.* **48**, 166–179.
Thode H. G., Monster J. and Dunford H. B. (1961) Sulphur isotope geochemistry. *Geochim. Cosmochim. Acta* **25**, 159–174.
Tudge A. P. and Thode H. G. (1950) Thermodynamic properties of isotopic compounds of sulphur. *Can. J. Res.* **28**, 567–578.
Turchyn A. V., Sivan O. and Schrag D. (2006) Oxygen isotopic composition of sulfate in deep sea pore fluid: evidence for rapid sulfur cycling. *Geobiology* **4**, 191–201.
Turchyn A. V., Brüchert V., Lyons T. W., Engel G. S., Balci N., Schrag D. P. and Brunner B. (2010) Kinetic oxygen isotope effects during dissimilatory sulfate reduction: a combined theoretical and experimental approach. *Geochim. Cosmochim. Acta* **74**, 2011–2024.
Turchyn A. V., Antler G., Byrne D., Miller M. and Hodell D. A. (2016) Sulfur metabolism evidenced from pore fluid isotope geochemistry at Site U1385. *Global Planet. Change* **141**, 82–90.
Wankel S. D., Bradley A. S., Eldridge D. L. and Johnston D. T. (2014) Determination and application of the equilibrium oxygen isotope effect between water and sulfite. *Geochim. Cosmochim. Acta* **125**, 694–711.
Wehrmann L. M., Templer S. P., Brunner B., Bernasconi S. M., Maignien L. and Ferdelman T. G. (2011) The imprint of methane seepage on the geochemical record and early diagenetic processes in cold-water coral mounds on Pen Duick Escarpment, Gulf of Cadiz. *Mar. Geol.* **282**, 118–137.
Wing B. A. and Halevy I. (2014) Intracellular metabolite levels shape sulfur isotope fractionation during microbial sulfate respiration. *Proc. Natl. Acad. Sci. U.S.A.* **111**, 18116–18125.
Wortmann U. G. (2008) Data report: $\delta^{34}S$ and $\delta^{18}O$ measurements of dissolved sulfate from interstitial water samples, IODP Expedition 311. In *Proc. IODP, 311* (eds. M. Riedel, T. S. Collett, M. J. Malone and the Expedition 311 Scientists). Integrated Ocean Drilling Program Management International, Inc., Washington, DC.
Wortmann U. G., Bernasconi S. M. and Böttcher M. E. (2001) Hypersulfidic deep biosphere indicates extreme sulfur isotope fractionation during single-step microbial sulfate reduction. *Geology* **29**, 647–650.
Wortmann U. G., Chernyavsky B., Bernasconi S. M., Brunner B., Böttcher M. E. and Swart P. K. (2007) Oxygen isotope biogeochemistry of pore water sulfate in the deep biosphere: dominance of isotope exchange reactions with ambient water during microbial sulfate reduction (ODP Site 1130). *Geochim. Cosmochim. Acta* **71**, 4221–4232.
Young E. D., Galy A. and Nagahara H. (2002) Kinetic and equilibrium mass-dependent isotope fractionation laws in nature and their geochemical and cosmochemical significance. *Geochim. Cosmochim. Acta* **66**, 1095–1104.
Zeebe R. E. (2010) A new value for the stable oxygen isotope fractionation between dissolved sulfate ion and water. *Geochim. Cosmochim. Acta* **74**, 818–828.
Zerkle A. L., Kamyshny A., Kump L. R., Farquhar J., Oduro H. and Arthur M. A. (2010) Sulfur cycling in a stratified euxinic lake with moderately high sulfate: constraints from quadruple S isotopes. *Geochim. Cosmochim. Acta* **74**, 4953–4970.

Associate editor: David Johnston